Published for SISSA by Springer

Received: *February 28, 2025*
Accepted: *May 19, 2025*
Published: *June 19, 2025*

Collinear and TMD distributions with dynamical soft-gluon resolution scale

F. Hautmann[a,b] **L. Keersmaekers**[a] **A. Lelek**[a] **S. Sadeghi Barzani**[a,c] **and S. Taheri Monfared**[d]

[a] *Universiteit Antwerpen, B 2020 Antwerpen, Belgium*
[b] *University of Oxford, Oxford OX1 3PU, U.K.*
[c] *Shahid Beheshti University, Tehran, Iran*
[d] *Deutsches Elektronen-Synchrotron DESY, Germany*

E-mail: francesco.hautmann@physics.ox.ac.uk, lissa.keersmaekers@uantwerpen.be, aleksandra.lelek@uantwerpen.be, safura.sadeghi67@gmail.com, taheri@mail.desy.de

Abstract: Soft-gluon resolution scales characterize parton branching Monte Carlo implementations of the evolution equations for parton distribution functions in Quantum Chromodynamics (QCD). We examine scenarios with dynamical, i.e., branching-scale dependent, resolution scale, and discuss physical implications for both collinear and transverse-momentum dependent (TMD) distributions. We perform the first determination of parton distributions with dynamical resolution scale, at next-to-leading order (NLO) in perturbation theory, from fits to precision deep-inelastic scattering measurements from HERA. We present an application of TMD distributions with dynamical resolution scale to Drell-Yan lepton-pair transverse momentum spectra at the LHC and lower-energy experiments, and comment on the extraction of non-perturbative intrinsic-k_T parameters from Drell-Yan data at small transverse momenta.

Keywords: Parton Distributions, Parton Shower

ArXiv ePrint: 2502.19380

https://doi.org/10.1007/JHEP06(2025)192

Contents

1 Introduction

The ever increasing precision of experimental measurements at present and future particle colliders [1–5] poses high demands on the performance of parton shower Monte Carlo event generators [6], which are essential to provide realistic event simulations and guide collider-physics analyses.

A long-standing issue in the use of QCD branching algorithms for parton showering in hadronic collisions concerns the treatment of parton distribution functions (PDFs), and more precisely the possible systematic bias induced by the potential mismatch between the (backward) shower evolution of the initial state [7, 8] and the PDF evolution equations [9–11].

In fact, on one hand shower algorithms make use of PDFs obtained from global fits to experimental data based on the evolution equations [9–11]; on the other hand, they incorporate features which are not present in these evolution equations and can give rise to potential differences. These may come from the choice of the ordering variable in the branching algorithm; the scale in the strong coupling α_s, and in particular the dependence of the coupling on the kinematics at each emission vertex in the parton decay chain; the showering scale q_0, representing the minimum transverse momentum with which any parton emitted in the partonic cascade can be resolved. As a result, even if at a given mass scale the PDF from global fit and the PDF used in the shower coincide, a possible mismatch may arise at a different mass scale due to evolution. See e.g. [12–31] for a sample of works which have investigated PDF issues in shower event generators.

In particular, the showering scale q_0 implies, by energy-momentum conservation, an upper bound on the fraction z of longitudinal momentum transferred at each emission. This

JHEP06(2025)192

defines, for any shower algorithm, a resolution scale in z for the soft gluons emitted in the branching. No such upper bound in z, in contrast, enters the PDFs which are extracted from global fits based on "inclusive" evolution equations [9–11], and used in the shower. See [22, 28, 30] for recent studies focusing on soft-gluon resolution effects.

An additional systematic effect arises from the transverse momentum recoils along the parton decay chain. Kinematic reshuffling transformations are employed to deal with the recoils in shower Monte Carlo generators [32–37]. This gives rise to shifts in the longitudinal momentum fractions z [38, 39], which can bias the use of PDFs in the shower generators, and ultimately even affect the soft-gluon region. An alternative method for incorporating transverse momentum recoils in branching algorithms is to bring in transverse momentum dependent (TMD) PDFs [40–42]. Through TMD PDFs, one can take into account consistently both the transverse momenta produced in the shower evolution and the nonperturbative "intrinsic" transverse momentum distributions characterizing hadronic states at low mass scales. From this perspective, the longitudinal-shift effect observed in [38, 39] due to the transverse recoils underlines the potential interplay of TMD dynamics with the soft-gluon resolution scale in z, and in particular with the systematics possibly induced by the use of collinear PDFs in parton showers.

The parton branching (PB) approach proposed in refs. [22, 43, 44], is designed to consistently treat both collinear and TMD distributions. As noted earlier, any branching algorithm will be characterized by the choices of the ordering variable, the scale in the strong coupling α_s, the soft-gluon resolution scale. As regards ordering variables, by examining transverse momentum, virtuality and angle ref. [43] finds that, while all three can be made to work for the case of collinear PDFs, the extension to TMDs can only be carried through in a well-prescribed manner by using angular ordering. As regards the strong coupling, by examining the branching scale and the emitted transverse momentum as scales in α_s it is found that, while both choices are able to describe inclusive deep inelastic scattering (DIS) structure functions [44], it is only the coupling evaluated at the transverse-momentum scale which is able to describe the Drell-Yan (DY) di-lepton transverse momentum distributions [45, 46] at small transverse momenta, and the di-jet azimuthal correlations [47, 48] at large azimuthal angles.

As regards the soft-gluon resolution scale, the PB approach [22, 43] can be applied either with a fixed (i.e., constant) resolution scale or with a running (i.e., branching-scale dependent, or "dynamical" [49]) resolution scale. These two scenarios have relevant implications for both theoretical and phenomenological aspects. On the theory side, the former scenario, once it is combined with the strong coupling evaluated at the branching scale, gives, upon integration over all transverse momenta, the DGLAP [9–11] evolution equations [43]. The latter scenario, once it is combined with the strong coupling evaluated at the emitted transverse momentum scale, gives, upon integration over all transverse momenta, the CMW [8, 50, 51] coherent-branching equations [49].

On the phenomenology side, the PB TMD approach with a fixed soft-gluon resolution scale and strong coupling at the transverse momentum scale has been successfully applied to simultaneously describe DIS inclusive structure functions [44] and DY transverse momentum distributions [45, 46, 52]. In particular, it has been used to make a determination of the nonperturbative "intrinsic" transverse-momentum parameter [52] from fits to DY experimental

JHEP06(2025)192

measurements across a wide range in DY mass and center-of-mass energy. This determination features a distinctive energy behavior of the intrinsic transverse-momentum at variance with determinations from tuning [53–58] of parton shower Monte Carlo generators [32–35]. We discuss these intrinsic-k_T studies (and their possible interpretation in terms of Sudakov effects [59–61]) later in section 2.2.

Phenomenological implications of PB TMD scenarios with dynamical soft-gluon resolution scale, on the other hand, have not yet been explored. It is the purpose of the present paper to start such investigations. To this end, we analyze the precision DIS structure function data [62] and perform fits to these data using the implementation of the PB TMD approach in the open-source fitting platform `xFitter` [63, 64]. We investigate whether good χ^2 values can be achieved, at next-to-leading order (NLO) in perturbation theory, using dynamical resolution scales. We find that this is the case; thus, from the best fit we extract for the first time collinear and TMD PDF sets with dynamical resolution scales. Similarly to the case of fixed resolution in [44], we provide the dynamical-resolution set including experimental and model uncertainties.

Next, we turn to DY transverse momentum spectra. Using the NLO PB sets extracted from DIS fits, we compute theoretical predictions for DY transverse momentum by applying the method [45] to match NLO DY matrix elements, obtained from the MADGRAPH5_AMC@NLO program [65] (denoted hereto as MCatNLO), with PB TMD parton distributions and parton showers implemented in the Monte Carlo event generator Cascade3 [66]. By comparing these predictions with the measurements [67] of DY transverse momentum at the Large Hadron Collider (LHC), we illustrate that a good description of DY p_T can be obtained with dynamical resolution scale, and perform a fit of the intrinsic transverse momentum parameter. This is the first extraction of intrinsic k_T using the PB TMD approach in the presence of dynamical resolution scales. We further perform fits to DY transverse momentum measurements from lower-energy experiments at Tevatron, RHIC and fixed target, obtaining a good description of the data and extracting the intrinsic transverse momentum parameter at different energies.

The collinear and TMD distributions determined from the DIS and DY analyses presented in this paper have wide applicability. First, the ability to properly describe inclusive DIS structure functions in a scenario with dynamical resolution scale (that is, "shower-like") is an important new result. The collinear PDFs with dynamical resolution scale extracted from DIS fits in this paper are suitable for use in shower Monte Carlo event generators.

Second, this paves the way for investigations, in the same framework, of non-inclusive observables describing the detailed structure of DIS final states both at HERA [68, 69] and at future lepton-hadron colliders [2, 4]. Monte Carlo event generators for DIS are currently being developed [25, 70]. A distinctive feature characterizing the framework of the present paper is the ability to simultaneously describe the inclusive DIS structure functions and non-inclusive DIS final states. The Cascade parton-shower Monte Carlo [66, 71] may be used for these applications (see e.g. [72, 73] for earlier results on DIS jets).

Third, the extraction of the intrinsic-k_T distribution in TMD PDFs performed in this paper from DY transverse momentum measurements can help elucidate the role of the soft-gluon resolution scale and nonperturbative Sudakov form factor [59, 60] in determining the energy dependence of the transverse-momentum Gaussian width [52, 53].

JHEP06(2025)192

The paper is organized as follows. In section 2 we briefly review the PB TMD formalism, discussing the evolution equations, the nonperturbative contributions and current results on the extraction of intrinsic-k_T parameters from experimental measurements. In section 3 we perform our fits to precision DIS data using dynamical resolution scales. We present results for integrated and TMD distributions, and discuss their dependence on the scale of the minimum transverse momentum for resolved parton emission. In section 4 we describe the application of the TMD distributions with dynamical resolution scale to DY transverse momentum spectra. We give conclusions in section 5.

2 Branching evolution

The analysis performed in this paper is based on the formulation of the PB TMD method given in refs. [43, 49]. We refer to these papers for the description and details of the method. This section provides a short recap of its main elements, concentrating on the features which will be central to the work presented in the following sections.

Subsection 2.1 is devoted to discussing the TMD branching evolution and its phase space in terms of two branching variables: the branching scale μ (which is related to the kinematic variables according to the ordering condition, e.g., angular ordering) and the longitudinal momentum fraction z (which is related to the rapidity of the radiated partons); or, alternatively, the longitudinal fraction z and the radiated transverse momentum $q_\perp$.

In this subsection we introduce the running, or dynamical, resolution scale $z_{\rm dyn}(\mu)$. This characterizes the rapidity evolution in the branching. We illustrate three relevant transverse-momentum scales in the branching: the intrinsic transverse momentum parameter q_s, describing the Gaussian width of the TMD distribution at low evolution scales; the minimum transverse momentum q_0 with which parton emissions can be resolved, representing the showering scale in the parton cascade associated with the evolution; the transverse-momentum scale q_c entering the strong coupling α_s according to the angular ordering [51, 74, 75] and "pre-confinement" picture [75, 76]. The scale q_c is of the same order as q_0, but it is conceptually distinct from it, and it does not necessarily have the same numerical value.

Subsection 2.2 summarizes recent determinations of the intrinsic transverse momentum parameter q_s from experimental DY measurements at small transverse momenta. Here we compare results obtained using the PB TMD method [52] and results obtained from the tuning of collinear shower Monte Carlo generators [53]. We comment on the role of the showering scale and soft-gluon resolution in this comparison. This discussion provides a further motivation for the investigations of the running, dynamical resolution scale which will follow in the next sections.

2.1 PB TMD evolution equations and nonperturbative contributions

The PB approach [22, 43] gives TMD evolution equations of the schematic form

$$\begin{aligned} A_a(x,\mathbf{k},\mu^2) = {} & \Delta_a(\mu^2,\mu_0^2)A_a(x,\mathbf{k},\mu_0^2) \\ & + \sum_b \int \frac{\mathrm{d}^2\boldsymbol{\mu}'}{\pi\mu'^2} \int \mathrm{d}z\ \mathcal{E}_{ab}[\Delta; P^{(R)}; \Theta] A_b(x/z, \mathbf{k} + a(z)\boldsymbol{\mu}', \mu'^2)\ , \end{aligned} \tag{2.1}$$

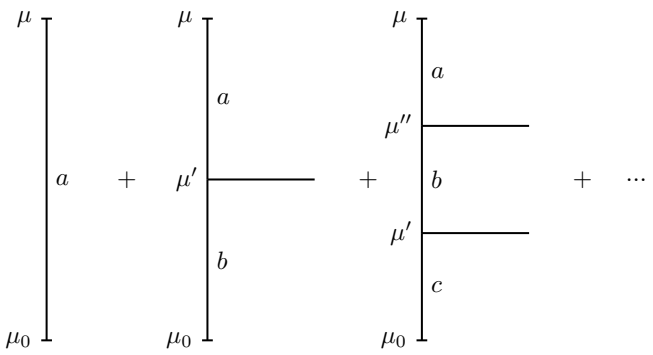

Figure 1. Solution of the branching equation by iteration.

where $A_a(x, \mathbf{k}, \mu^2)$ is the TMD distribution of flavor a, carrying the longitudinal momentum fraction x of the hadron's momentum and transverse momentum $\mathbf{k}$ at the evolution scale μ; $\Delta_a(\mu^2, \mu_0^2)$ is the Sudakov form factor for the no-emission probability of flavor a from scale μ_0 to scale μ; $\mathcal{E}_{ab}$ are the evolution kernels, which are given as functionals of the Sudakov form factors Δ_a and of the real-emission splitting functions P_{ab}^R [43], and depend on phase-space constraints collectively denoted by Θ in eq. (2.1). The functions that appear in the evolution kernels can be computed as perturbation expansions in powers of the strong coupling α_s. The explicit expressions of these expansions for all flavor channels are given to two-loop order in ref. [43].

The evolution in eq. (2.1) is expressed in terms of two branching variables, z and $\boldsymbol{\mu}'$: z is the longitudinal momentum transfer at the branching, while $\mu' = \sqrt{\boldsymbol{\mu}'^2}$ is the mass scale at which the branching occurs. The parton decay chain arising from the evolution is pictured in figure 1 in terms of multiple branchings, $i = 1, 2, \ldots$. The longitudinal momentum transfers z_i control the rapidities y_i of the partons emitted along the parton decay chain, $y_i \sim \ln 1/z_i$. The mass scales of the branching μ_i', on the other hand, are related to the branching's kinematic variables according to the ordering condition.[1] This is specified by the function $a(z)$ in the last factor on the right hand side of eq. (2.1). Transverse momentum ordering, virtuality ordering and angular ordering are examined in refs. [22, 43]. The angular-ordered branching is motivated by the treatment of the endpoint region in the TMD case [43, 81]. For angular ordering, one has $a(z) = 1 - z$, and the branching scale μ_i' is related to the transverse momentum $q_{\perp,i}$ of the parton emitted at the i-th branching by

$$\mu_i' = q_{\perp,i}/(1 - z_i). \tag{2.2}$$

The initial evolution scale in eq. (2.1) is denoted by μ_0, which is taken to be $\mu_0 > \Lambda_{\mathrm{QCD}}$. It is usually of order $\mu_0 \sim \mathcal{O}(1\,\mathrm{GeV})$. The distribution $A_a(x, \mathbf{k}, \mu_0^2)$ at scale μ_0 in the first term on the right hand side of eq. (2.1) represents the intrinsic k_T distribution. This is a nonperturbative boundary condition to the evolution equation, which can be arrived at from comparisons of theory predictions to experimental data. Following previous applications of the PB TMD method [44, 52], for simplicity in the calculations that follow we will parameterize

[1] Rapidity and mass evolution for TMD distributions can also be formulated in a CSS [77, 78], rather than PB, approach. See e.g. [79, 80].

JHEP06(2025)192

$\mathcal{A}_a(x, \mathbf{k}, \mu_0^2)$ in the form

$$\mathcal{A}_a(x, \mathbf{k}, \mu_0^2) = f_a(x, \mu_0^2) \cdot \exp\left(-|k_T^2|/2\sigma^2\right)/(2\pi\sigma^2) \,, \tag{2.3}$$

with $|k_T^2| = \mathbf{k}^2$ and the width of the Gaussian transverse-momentum distribution given by $\sigma = q_s/\sqrt{2}$, independent of parton flavor and x, where q_s is the intrinsic-k_T parameter.

As noted earlier, the evolution kernels $\mathcal{E}_{ab}$ and the Sudakov form factors Δ_a in eq. (2.1) depend on kinematic constraints providing the phase space of the branchings along the parton cascade. These can be represented, using the "unitarity" picture of QCD evolution [51], by separating resolvable and non-resolvable branchings in terms of a resolution scale to classify soft-gluon emissions [22]. Employing the branching variables (z, μ'), applications of the PB TMD method have either taken the soft-gluon resolution parameter to be a finite constant close to the kinematic limit $z = 1$ or allowed for a running, μ'-dependent resolution. In the first case, one has the fixed soft-gluon resolution parameter

$$z_M = 1 - \varepsilon \;\; , \tag{2.4}$$

where ε is chosen to be a constant $\ll 1$. In the second case, let q_0 be the minimum transverse momentum with which any emitted parton can be resolved, so that $q_{\perp,i} \geq q_0$ for any i. Using the angular-ordering relation in eq. (2.2), the condition for resolving soft gluons is given by $z_i \leq z_M(\mu_i')$, where the running soft-gluon resolution parameter is

$$z_M(\mu') = 1 - q_0/\mu' \equiv z_{\rm dyn} \;\; . \tag{2.5}$$

Eq. (2.5) defines the dynamical resolution scale $z_{\rm dyn}$ associated with the angular ordering [8, 49–51]. The transverse momentum scale q_0 represents the showering scale, down to which resolved parton emissions take place. Like the scale μ_0, the showering scale q_0 lies in the region above $\Lambda_{\rm QCD}$, and is usually of order $q_0 \sim \mathcal{O}(1\,{\rm GeV})$.

Figure 2 depicts the resolvable and nonresolvable regions in the partonic branching phase space [49], mapped on the branching variables (z, μ') in the left hand side panel and on $(q_\perp, z)$ in the right hand side panel. The pictures refer to the case in which the ratio of the showering scale q_0 and starting evolution scale μ_0 is smaller than $1 - x$, $q_0/\mu_0 < 1 - x$. Analogous pictures are given in ref. [49] for the complementary case $q_0/\mu_0 \geq 1 - x$.

The green-colored line in either panel (on the left or on the right of figure 2) represents the starting evolution scale, $\mu' = \mu_0$, at which the nonperturbative intrinsic k_T distribution in eq. (2.3) is defined. The red-colored line in the left hand side panel represents the dynamical, running resolution scale $z_{\rm dyn}$ in eq. (2.5); equivalently, the red-colored line in the right hand side panel corresponds to $q_\perp = q_0$, where q_0 is the showering scale. The yellow-colored domains in either panel correspond to the resolvable radiation region, which is treated perturbatively in eq. (2.1). The grey-colored domains in either panel, on the other hand, involve infrared-sensitive radiative processes with $z > z_{\rm dyn}$ and small transverse momenta below the scale q_0, requiring the modeling of nonperturbative contributions.

Both the green-colored line and grey-colored region, in either panel of figure 2, are thus controlled by nonperturbative effects. The former corresponds to the intrinsic TMD distribution, and the latter corresponds to the nonperturbative component of the Sudakov

JHEP06(2025)192

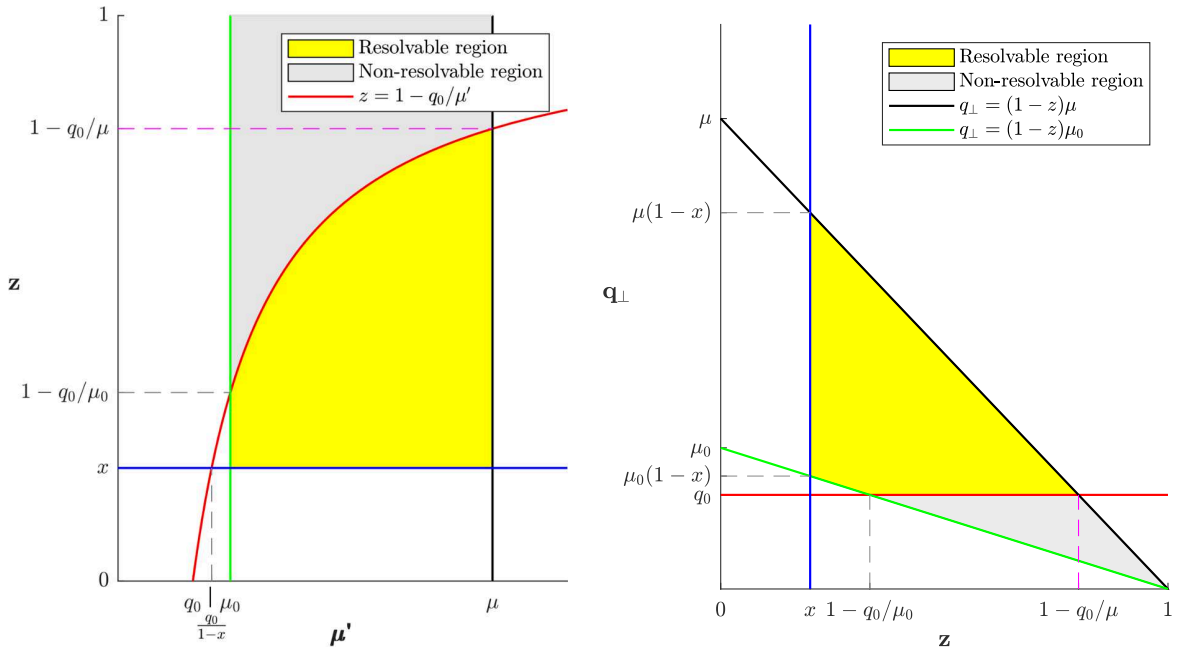

Figure 2. The regions of resolvable and non-resolvable branchings (from ref. [49]), for $q_0/\mu_0 < 1 - x$, mapped on the (μ', z) plane (left) and the $(z, q_\perp)$ plane (right).

form factor. The former may be viewed as a boundary condition to the evolution, while the latter as an integral part of the evolution.[2]

A possible approach to applying the PB TMD method is to use fixed resolution scale z_M as in eq. (2.4), and extend the evolution kernels $\mathcal{E}_{ab}$ of eq. (2.1) into the grey-colored regions in figure 2 with a suitable treatment of the strong coupling α_s [44–46, 52]. Two common scenarios for α_s are the following: i) the coupling is evaluated at the branching scale, $\alpha_s = \alpha_s(\mu'^2)$; ii) the coupling is evaluated at the transverse momentum of the emission, $\alpha_s = \alpha_s(q_\perp^2) = \alpha_s(\mu'^2(1-z)^2)$. Case i) corresponds to DGLAP evolution [9–11] , while case ii) corresponds to angular ordering, e.g. CMW evolution [8, 50].[3] While either one can be used for totally inclusive cross sections [44], case ii) is required for the description of differential transverse-momentum distributions and angular correlations [45–48].

We observe in figure 2 that the grey-colored regions do not require any further treatment of the strong coupling in case i) (as $\mu' \geq \mu_0$), while they do in case ii) (as $q_\perp \lesssim q_0$). To this end, the strong coupling is modeled according to a "pre-confinement" picture [75, 76] as

$$\alpha_s = \alpha_s(\max(q_c^2, q_\perp^2)), \tag{2.6}$$

where q_c is a semi-hard scale on the order of the GeV.

This approach, characterized by the fixed z_M in eq. (2.4) and the strong coupling in eq. (2.6), has been shown to give rise to a successful description of inclusive DIS structure

[2] An analogous picture can be given in the CSS [77, 78] context: see e.g. [80, 82]. Nonperturbative Sudakov effects, corresponding to the grey-colored regions of figure 2, are then embodied by the rapidity evolution Collins-Soper [83, 84] kernel.

[3] Angular ordering is also used in the KMR approach [85, 86]. See [49, 87–92] for recent discussions of both infrared and ultraviolet issues in this case.

JHEP06(2025)192

functions, DY transverse-momentum distributions and di-jet angular correlations [44–47]. In fact, it has been used to make a determination [52] of the intrinsic-k_T parameter q_s in eq. (2.3) from fits to DY experimental measurements across a wide range in masses and center-of-mass energies.

In the present paper, we explore a different approach. Namely, we take the running resolution scale z_M as in eq. (2.5), and investigate its implications for the description of DIS and DY processes. On one hand, this is of interest in its own right, as it allows one to investigate the role of the boundary between resolvable and unresolvable branchings, and deepen the study of nonperturbative effects. For instance, the extraction of the intrinsic-k_T distribution is expected to be sensitive to the modeling of soft-gluon resolution [52]. On the other hand, from the standpoint of general-purpose shower Monte Carlo generators [32, 34] the set-up with the running resolution scale (2.5) may be helpful in investigating open issues about the use of PDFs in collinear showers [28, 30] and the showering scale.

We will proceed in a similar fashion to what is done in the literature for the fixed-z_M case. That is, we first apply the dynamical-scale scenario in eq. (2.5) to DIS: in section 3 we perform fits to precision data for DIS structure functions, determining new collinear and TMD PDF sets. These results are timely, given the currently planned DIS experiments [2, 4] (with accompanying efforts to develop new Monte Carlo event generators for DIS [25, 70]). Next, we apply the newly determined TMD distributions to DY transverse momentum spectra: in section 4 we compare theoretical predictions obtained using dynamical resolution scale with experimental measurements [67] of DY transverse momentum, and examine the intrinsic-k_T parameter q_s. This can be regarded as a first step toward a full fit covering DY data from experiments at all available energies and DY masses.

Before we move on to this in sections 3 and 4, we conclude the present section with an overview of the current status of extractions of intrinsic transverse momentum from DY data, based on PB TMD calculations [52, 93] on one hand, and on tuning of general-purpose Monte Carlo generators [53, 54] on the other hand. The comparison of the results from these analyses underlines the potential impact of the showering scale and soft-gluon resolution on intrinsic k_T distributions. It thus reinforces the motivation for the studies of dynamical resolution scale in the sections that follow.

2.2 Extractions of intrinsic transverse momentum from data

Recently, two analyses of intrinsic transverse momentum distributions from DY measurements at small transverse momenta have been carried out which highlight features of the approach described in the previous subsection and of collinear showering approaches. The two analyses are that of ref. [52], based on the implementation of the PB TMD method in the Monte Carlo event generator Cascade3, and that of the CMS Collaboration [53, 54], based on underlying-event tunes of Monte Carlo event generators Pythia8 and Herwig7. In this subsection we summarize and compare the results.

Ref. [52] uses the PB TMD approach [22, 43] described above in this section, with the fixed z_M in eq. (2.4), angular-ordered α_s in eq. (2.6), and TMD PDF set PB-NLO-2018-Set2 [44]. It computes predictions for DY transverse momentum distributions by using the technique [45] for matching DY matrix elements at NLO obtained from the MCatNLO

JHEP06(2025)192

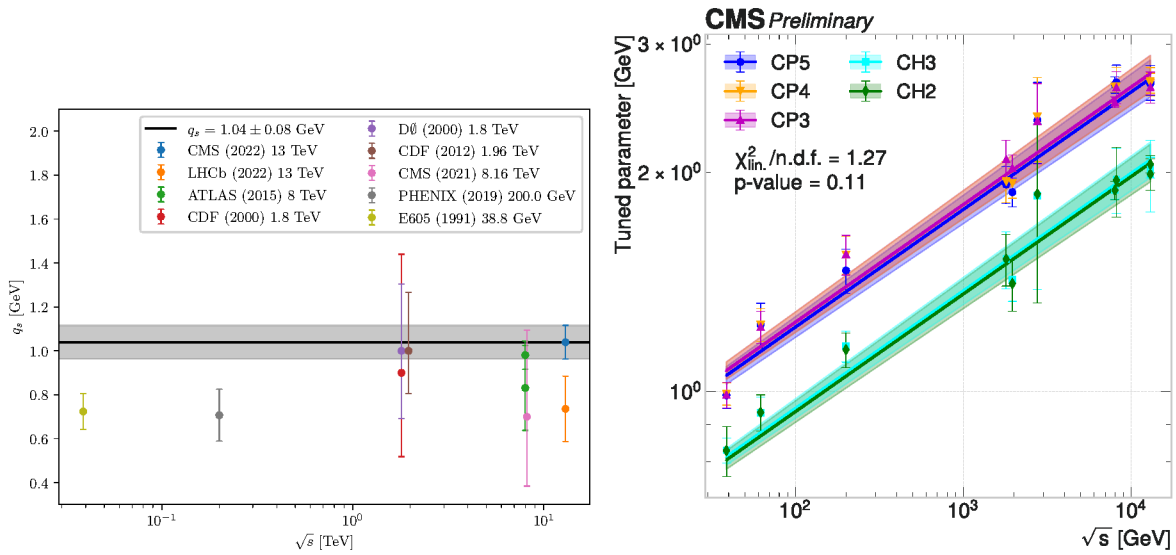

Figure 3. Extraction of intrinsic k_T parameter from measurements of DY transverse momentum distributions at varying center-of-mass energies. The plot on the left hand side is taken from ref. [52], and is based on predictions using the TMD parton branching implemented in the Monte Carlo event generator CASCADE3. The plot on the right hand side is taken from ref. [54], and is based on underlying-event tunes of the Monte Carlo event generators PYTHIA8 (CP3, CP4, CP5) and HERWIG7 (CH2, CH3).

program [65] with TMD parton distributions and showers implemented in the Monte Carlo generator CASCADE3 [66]. As discussed earlier, in this approach TMD distributions are systematically introduced and evolved, and at the starting scale of evolution they are parameterized (see eq. (2.3)) and fitted to experimental data. The analysis [52] extracts the intrinsic k_T parameter q_s by performing fits to DY transverse momentum data [67, 94–101], including a detailed treatment of statistical, correlated and uncorrelated uncertainties.[4] The CMS data [67] at center of mass energy $\sqrt{s} = 13\,\text{TeV}$ cover DY invariant masses from 50 GeV to 1 TeV. The other data cover energies from 13 TeV down to 38 GeV. The results [52] for q_s versus energy $\sqrt{s}$ are reported in figure 3 in the left hand side panel.

The CMS analysis [53, 54] is based on NLO predictions from MCatNLO [65] matched with HERWIG7 [32] and with PYTHIA8 [35] parton showers and underlying event models. It uses the HERWIG7 tunes CH2 and CH3 [57] and PYTHIA8 tunes CP3, CP4 and CP5 [55] for the underlying event. Although TMD distributions are not used, both the HERWIG7 and PYTHIA8 calculations introduce intrinsic k_T distributions parameterized as Gaussian distributions with tunable parameters. The analysis [53, 54] extracts the intrinsic k_T parameter from DY transverse momentum measurements at the LHC, Tevatron, RHIC and fixed-target experiments. The results [54] for the intrinsic k_T parameter versus energy $\sqrt{s}$ are reported in figure 3 in the right hand side panel.

The left and right panels of figure 3 indicate a striking difference in the energy dependence of the intrinsic k_T parameter between the TMD parton branching and collinear shower

[4]It is shown in refs. [93, 102] that an extraction of the q_s parameter similar to that in ref. [52] can be carried out by using, rather than the differential cross section, simpler observables defined from ratios of p_T bins in a coarse-grained binning scenario.

JHEP06(2025)192

calculations. While the right panel shows a strong rise with energy,[5] no strong rise is found in the left panel.

It is suggested in [52] that this difference in the energy behavior of the intrinsic k_T can be attributed to nonperturbative Sudakov effects [59, 60] arising from the region near the soft-gluon resolution boundary. With reference to figure 2, this means that different behaviors of intrinsic-k_T distributions along the green-colored line in figure 2 can reflect different treatments of soft radiative processes populating the grey-colored regions [49].[6]

In particular, the picture proposed in [52] suggests that the transition from the nearly-constant behavior of q_s with energy in the left panel of figure 3 to the power-like rise in the right panel of figure 3 can be related to the change in resolution scales from eq. (2.4) to eq. (2.5), and that this can be studied as a function of the showering scale q_0, entering the dynamical soft-gluon scale $z_{\rm dyn}$ in eq. (2.5).[7]

The potential interplay of q_s and q_0 provides an important motivation for the systematic studies of dynamical $z_{\rm dyn}$ which are at the center of this work.

3 Fits to DIS precision data with dynamical resolution scale

In this section we present the PB TMD fits to precision DIS structure function data [62] from HERA, using dynamical resolution scales. First results from these fits have appeared in [111]. The collinear and TMD PDFs obtained from the fits will be made available in the TMDlib library [112, 113].

3.1 Fit procedure and general settings

The software to fit PB distributions to data from cross sections' measurements within the `xFitter` package [63, 64] was developed in refs. [114–117] and further applied in ref. [44]. The fit procedure is based on the construction of kernels obtained from the Monte Carlo solution of the PB equation discussed in the previous section, and the use of TMD distributions as well as integrated TMD distributions (iTMD), resulting from the integration over transverse momenta of the TMDs. We refer the reader to the above-mentioned references [44, 114–117] for details on the fit procedure.

In what follows, we will apply this procedure with the only difference, compared to the above references, that the kernels will depend on the running soft-gluon resolution scale given by the dynamical z_M in eq. (2.5). We will perform fits for different values of the showering scale q_0 in eq. (2.5). We will use NLO splitting functions and two-loop running coupling α_s in the kernels, unless stated otherwise. We will set the scale q_c in the running coupling in eq. (2.6) equal to q_0, unless stated otherwise. The result of the fits will be the NLO determination of the initial distributions in eq. (2.3), parameterized at the starting scale μ_0 of the evolution.

[5] The rise of intrinsic k_T with energy observed in the right panel of figure 3 confirms earlier results obtained with Herwig [103] and Pythia [104].

[6] A related observation has been made in the context of CSS studies in ref. [80], by examining correlations between the TMD distribution (corresponding to the green-colored line in figure 2) and the Collins-Soper kernel (receiving nonperturbative contributions from the grey-colored regions in figure 2).

[7] The idea proposed in [52] is further explored in [105–110].

JHEP06(2025)192

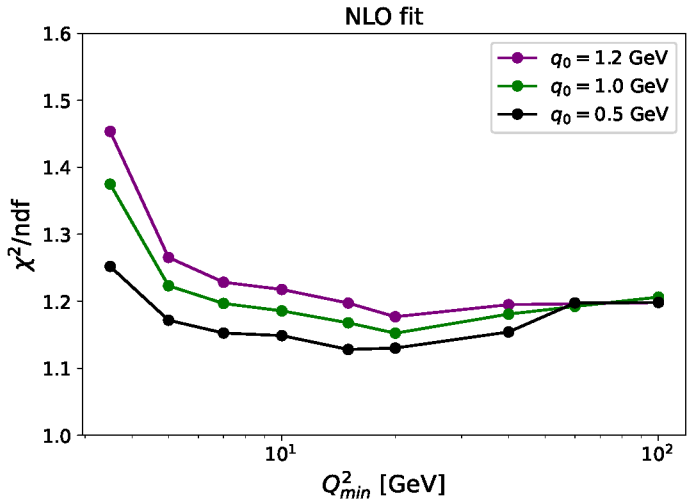

Figure 4. The χ^2/n.d.f. value of the NLO dynamical-z_M fit to DIS precision data [62] as a function of the minimum Q^2 of the data included in the fit, for different values of q_0.

Following the strategy of ref. [44], adapted from the HERAPDF2.0 fits [62], the initial parameterizations have the form

$$\begin{aligned} xg(x) &= A_g x^{B_g}(1-x)^{C_g} - A'_g x^{B'_g}(1-x)^{C'_g} , \\ xu_v(x) &= A_{u_v} x^{B_{u_v}}(1-x)^{C_{u_v}}(1+E_{u_v}x^2) , \\ xd_v(x) &= A_{d_v} x^{B_{d_v}}(1-x)^{C_{d_v}} , \\ x\overline{U}(x) &= A_{\overline{U}} x^{B_{\overline{U}}}(1-x)^{C_{\overline{U}}}(1+D_{\overline{U}}x) , \\ x\overline{D}(x) &= A_{\overline{D}} x^{B_{\overline{D}}}(1-x)^{C_{\overline{D}}} , \end{aligned} \tag{3.1}$$

where the notation for parton distributions and parameters follows that of ref. [62]. Additional constraints are applied at the initial scale μ_0: $x\overline{U} = x\overline{u}$ and $x\overline{D} = x\overline{d} + x\overline{s}$. For the initial strange-quark distribution, we apply $x\overline{s} = f_s x\overline{D}$ with $f_s = 0.4$. We set $B_{\overline{U}} = B_{\overline{D}}$ and $A_{\overline{U}} = A_{\overline{D}}(1 - f_s)$. The normalization parameters A_{u_v}, A_{d_v}, A_g and $A_{g'}$ are constrained by the quark number and momentum sum rules. C'_g is fixed to 25 as in the HERAPDF2.0 set [62]. We use the same hard-scattering coefficient functions and we treat heavy flavors in the same way as was done in refs. [44, 62]. The intrinsic transverse momentum is generated from the Gaussian distribution with the width $\sigma = q_s/\sqrt{2}$ with $q_s = 0.5$ GeV if not written explicitly otherwise.

The fit is performed with the inclusive DIS data from the HERA H1 and ZEUS combined measurement [62] in the range of $3.5 < Q^2 < 50000$ GeV^2, $8 \cdot 10^{-5} < x < 0.65$. The number of data points included in the fit is 1131.

The χ^2 is calculated within the `xFitter` package. As in ref. [44], systematic shifts and the treatment of correlated and uncorrelated systematic uncertainties are included in the χ^2 definition. A total of 162 systematic uncertainties and uncertainties from the procedure of combining H1 and ZEUS data are treated as correlated.

The experimental uncertainties on the parton distributions are obtained by using the Hessian method [118], implemented in `xFitter`, with $\Delta\chi^2 = 1$. The model uncertainties

JHEP06(2025)192

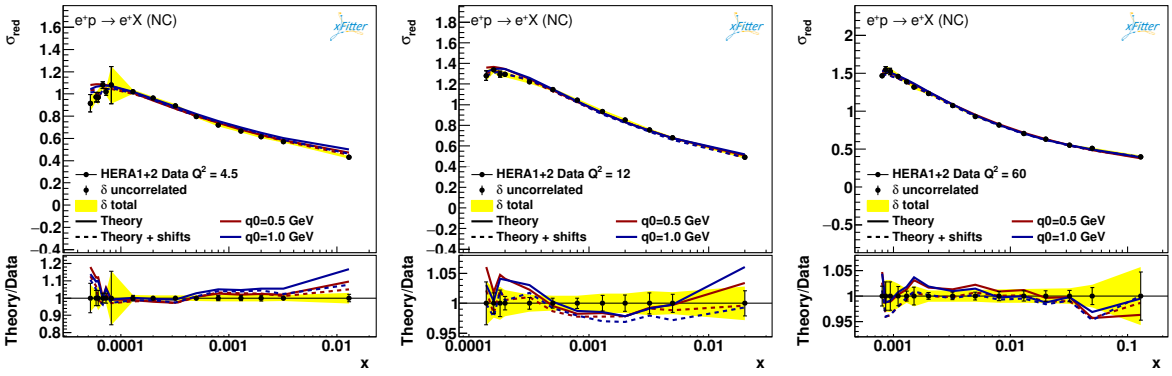

Figure 5. Predictions for the inclusive DIS reduced cross section obtained using dynamical z_M with $q_0 = 0.5$ GeV and $q_0 = 1.0$ GeV, compared to HERA data [62].

are obtained by varying the charm ($m_c = 1.41, 1.47, 1.53$ GeV) and the bottom mass ($m_b = 4.25, 4.5, 4.75$ GeV), and the starting evolution scale ($\mu_0^2 = 1.6, 1.9, 2.2$ GeV^2) where the numbers in brackets are the lower, central and upper values respectively.

Further refinements of these fits can be envisioned but are not included in the present study. For instance, one could imagine fitting the intrinsic-k_T scale q_s as well as the scale q_0. Also, one could study uncertainties due to the parameterization choice, and the impact of H1 and Zeus combined heavy-quark data [119, 120]. We leave these developments to future investigations.

3.2 Description of the data and fitted distributions

We now present the results of the PB fits with dynamical resolution scale, described in the previous subsection, at NLO. We present fits for three different values of the showering scale q_0: 1.2 GeV, 1 GeV and 0.5 GeV. We will refer to these fits as PB-NLO-2025-DynZm, with suffixes q0-1_2, q0-1_0, q0-0_5 and they will be available in TMDlib.

The values of χ^2/n.d.f. (number of degrees of freedom) for these three fits are as follows: 1.45 (for $q_0 = 1.2$ GeV); 1.37 (for $q_0 = 1$ GeV); 1.26 (for $q_0 = 0.5$ GeV).

To examine the behavior of the fits in different kinematic regions of Q^2, we also perform fits on data subsets characterized by different values of the lowest Q^2, $Q^2_{\rm min}$. The results for the χ^2/n.d.f. values are reported in figure 4 as a function of $Q^2_{\rm min}$, for the fits corresponding to the three different values of q_0.

Figure 4 shows that good χ^2 values are obtained from the NLO fits for all three values of q_0, throughout the kinematic range in Q^2. The χ^2 improves as q_0 decreases in the range of the chosen values. We will analyze this behavior further in the next two subsections, both by examining the impact of the perturbative order on the fit (through a comparison with leading-order (LO) fits in subsection 3.3) and by examining the role of the coupling α_s in eq. (2.6) in the low transverse momentum region (through a comparison with a fit keeping $q_c \neq q_0$ in subsection 3.4).

The description of the data for the inclusive-DIS reduced cross section is illustrated in figure 5 for the cases $q_0 = 0.5$ GeV and $q_0 = 1.0$ GeV. As expected from the results above, the differences between the sets do not influence very much the description of the inclusive-DIS

JHEP06(2025)192

$q_0 = 0.5$ GeV

	A	B	C	D	E	A'	B'	C'
xg	0.49	-0.10	0.86			-0.08	-0.22	25.0
xu_v	3.29	0.70	4.37		17.95			
xd_v	3.29	0.87	3.45					
$x\overline{U}$	0.16	-0.14	6.49	0.0				
$x\overline{D}$	0.27	-0.14	9.04					

$q_0 = 1.0$ GeV

	A	B	C	D	E	A'	B'	C'
xg	1.99	-0.19	7.37			0.72	-0.24	25.0
xu_v	4.54	0.74	5.43		17.12			
xd_v	2.35	0.72	3.69					
$x\overline{U}$	0.21	-0.09	7.83	4.56				
$x\overline{D}$	0.34	-0.09	6.17					

$q_0 = 1.2$ GeV

	A	B	C	D	E	A'	B'	C'
xg	4.89	-0.12	12.25			3.29	-0.09	25.000
xu_v	4.30	0.71	5.52		16.90			
xd_v	2.43	0.72	3.92					
$x\overline{U}$	0.24	-0.07	78.37	5.36				
$x\overline{D}$	0.40	-0.07	7.59					

Table 1. Parameter values of the fitted initial distributions for fits with $q_0 = 0.5,\ 1.0$ and 1.2 GeV.

data, and the quality of the different fits is similar. The results for the fitted parameters of the initial distributions are shown in table 1.[8]

In figure 6 the iTMD distributions corresponding to the three fits with the different values of q_0 are shown for several evolution scales and parton flavors. The result for the fit PB-NLO-2018-Set2 of ref. [44], which is based on fixed resolution scale z_M and $q_c = 1$ GeV, is shown as well and is used as a reference in the ratio plots. The distributions obtained with different q_0 values are different. Since the effect of z_M accumulates in each branching, the distributions differ also at high scales. For gluon, the differences are larger than for quarks. The gluon distribution in the fit with $q_0 = 0.5$ GeV is however similar to PB-NLO-2018-Set2.

In figure 7, experimental and model uncertainties of the fitted distributions are shown for the dynamical-z_M set with $q_0 = 1.0$ GeV, and compared to PB-NLO-2018-Set2. The differences between these two sets are generally larger than the uncertainty band from the fits. Also, the differences between the curves with different q_0 values from figure 6 are larger than the uncertainty band for $q_0 = 1.0$ GeV.

As discussed above, following the procedure in refs. [44, 114, 116] the TMD distributions are obtained from a convolution of the TMD kernel with the starting distribution. In figure 8 the TMD distributions as functions of the transverse momentum k_T are shown for gluon and

[8] One may note that for $q_0 = 0.5$ GeV the parameter D for $x\bar{U}$ is fixed to 0.0. The reason for this is that the fit with the default parameterization of eq. (3.1) resulted in a negative value of this parameter, leading to a negative quark distribution. To avoid it, the fit was repeated with $D = 0$ for $x\bar{U}$.

JHEP06(2025)192

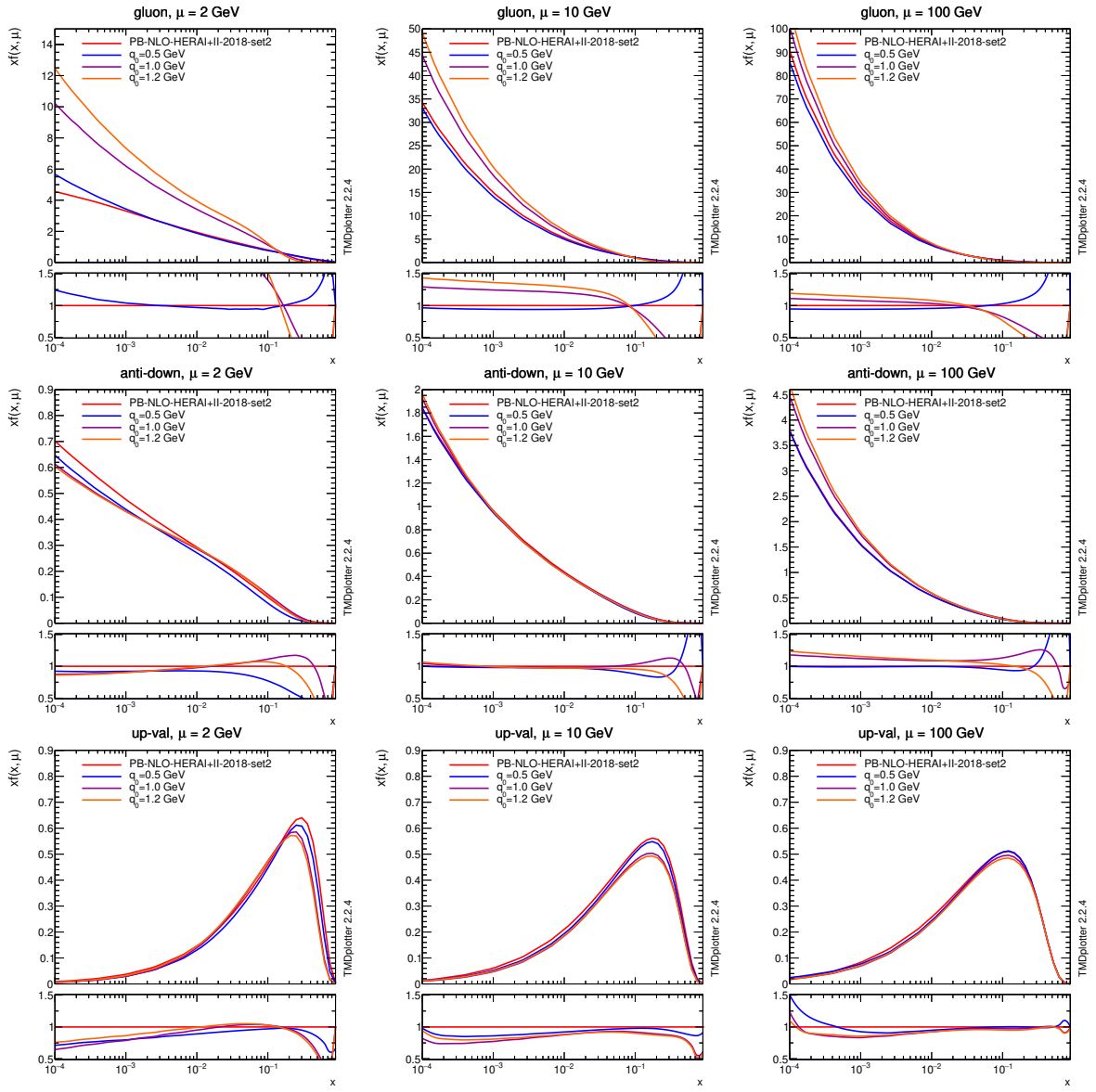

Figure 6. The iTMD distributions for different parton species as functions of x at $\mu = 2,\ 10,\ 100\,\text{GeV}$ obtained from the NLO dynamical-z_M fits with $q_0 = 0.5,\ 1.0$ and 1.2 GeV. The fixed-z_M set PB-NLO-2018-Set2 is included for comparison.

anti-down quark, at values of longitudinal momentum fractions $x = 0.1$ and 0.001 and at evolution scales $\mu = 10$ GeV and $\mu = 100$ GeV, for different q_0 values. PB-NLO-2018-Set2 is shown as well and is used as a reference on the ratio plots. The distributions obtained with different q_0 values differ especially in the low-k_T region. At larger k_T the shape of the distributions is similar. It is worth noting that for very low $|k_\perp| \approx 1$ GeV a dip may arise in the region of the minimal emitted transverse momentum due to the matching between the intrinsic transverse momentum and the transverse momentum generated by the evolution. The dip is less pronounced for lower q_0 values, when more branchings are generated. Similarly to the iTMD case, the result with $q_0 = 0.5$ GeV is quite similar to PB-NLO-2018-Set2.

JHEP06(2025)192

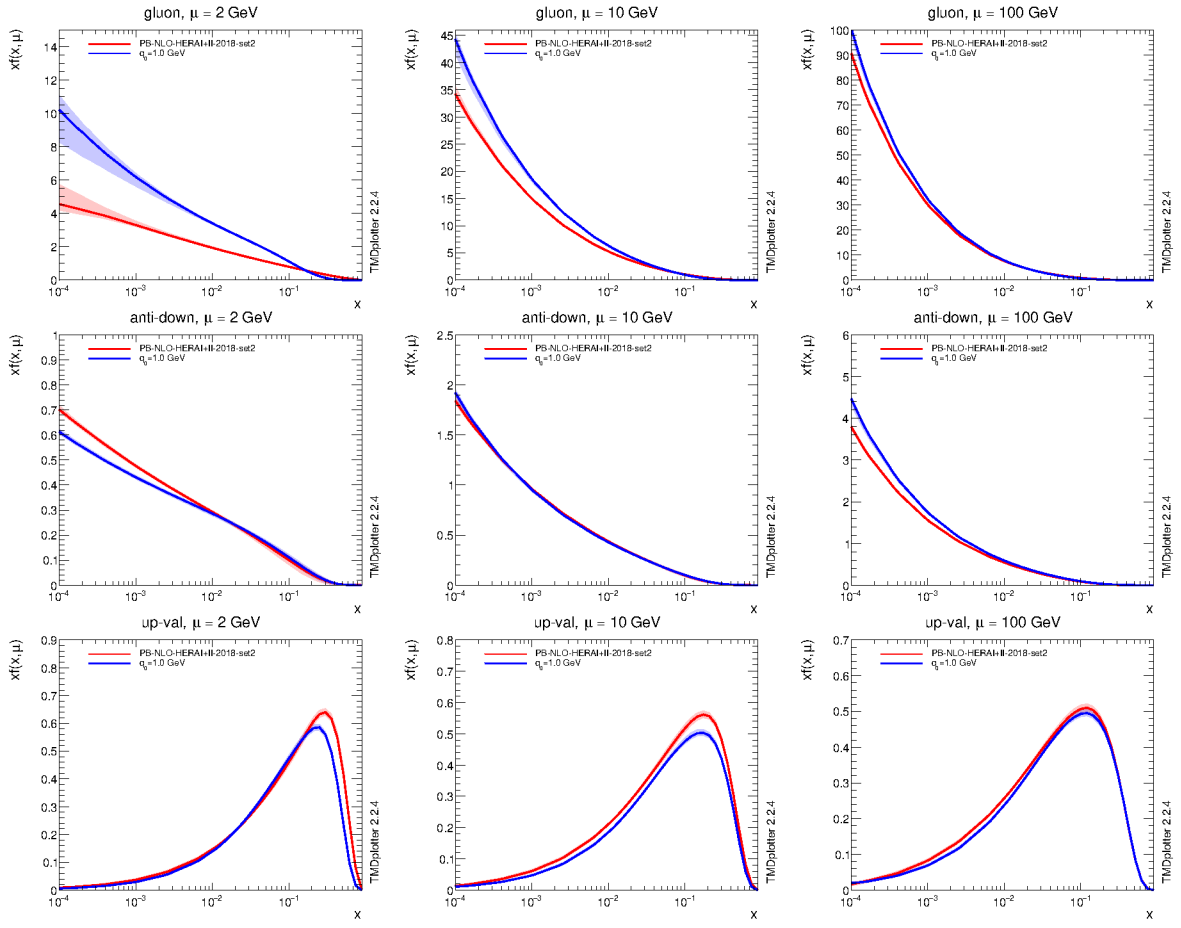

Figure 7. Experimental and model uncertainties of the iTMD distributions for gluon, down and up quark as functions of x at $\mu = 2,\ 10,\ 100$ GeV obtained from the dynamical-z_M fit with $q_0 = 1.0$ GeV. The fixed-z_M set PB-NLO-2018-Set2 is included for comparison.

In figure 9, the experimental and model uncertainty bands are shown as functions of k_T for the TMD distributions obtained from the fit with $q_0 = 1.0$ GeV. The PB-NLO-2018-Set2 result is also shown for comparison. Similarly to the iTMD case, the distributions are different, with the differences exceeding the uncertainty band.

3.3 Leading-order fits

We now present fits performed with the same approach as the ones in the previous subsection but at leading order (LO) in perturbation theory, that is, using LO splitting functions and hard-scattering matrix elements, and one-loop running coupling.[9] LO fits may be useful, given the potential application of dynamical z_M to parton showers using LO splitting functions. Besides, this study allows us to investigate the impact of perturbative order on DIS fits.

The results for the χ^2/n.d.f. values of the LO fits, corresponding to the three different values of q_0 as in the previous subsection, are reported in figure 10 as a function of $Q^2_{\min}$.

[9]For the LO fits, the parameterizations of the initial distributions are kept as in eq. (3.1) except for the gluon, for which, following discussions in [62, 64], we use a parameterization with three parameters instead of five.

JHEP06(2025)192

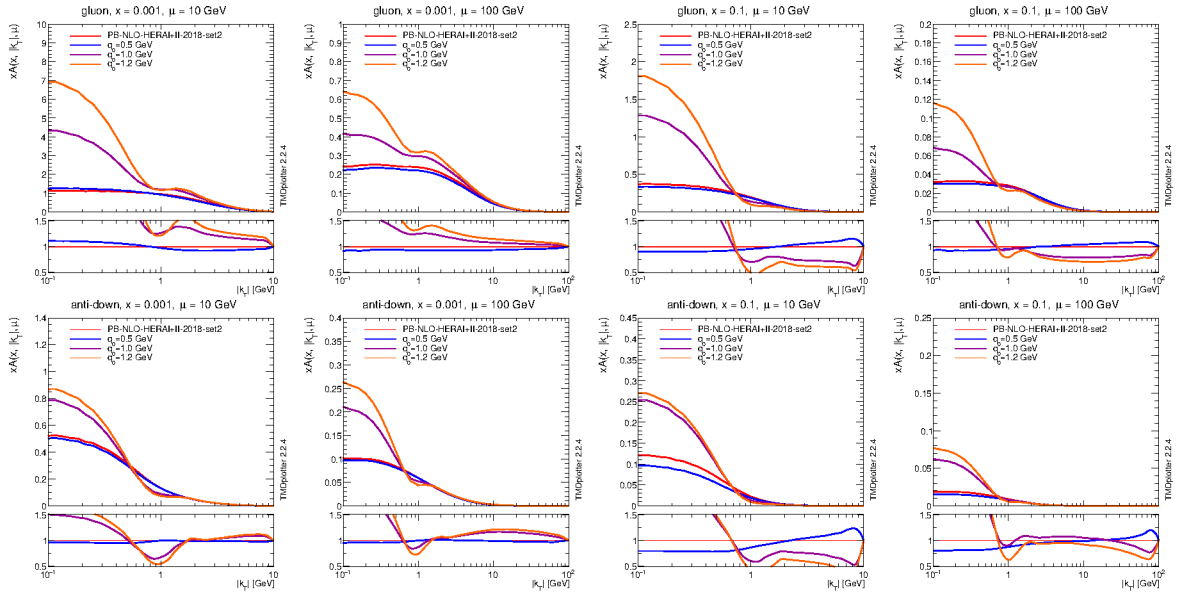

Figure 8. The k_T dependence of TMD distributions for gluon and anti-down quark obtained from the NLO dynamical-z_M fits with different q_0 values, for $\mu = 10$ and 100 GeV and $x = 0.001$ and 0.1. The fixed-z_M set PB-NLO-2018-Set2 is included for comparison.

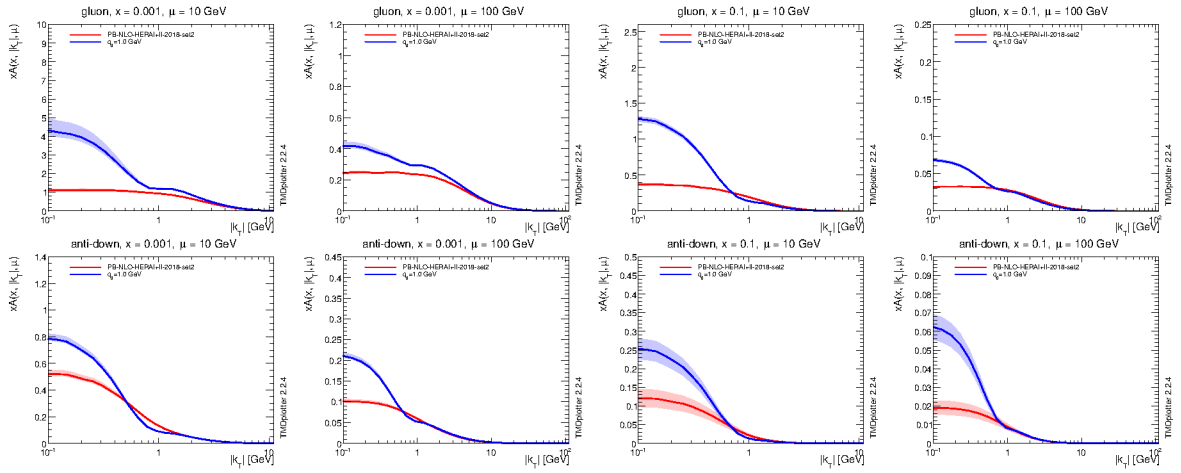

Figure 9. Experimental and model uncertainties for TMD distributions of gluon and anti-down quark as functions of k_T at $\mu = 10$ and 100 GeV and $x = 0.001$ and 0.1, obtained from the dynamical-z_M fit with $q_0 = 1$ GeV. The fixed-z_M set PB-NLO-2018-Set2 is included for comparison.

By comparing figure 10 with figure 4, we see that the χ^2/n.d.f. is significantly better in the NLO case than the LO case for all q_0 values, and that the difference among fits with different q_0 values is stronger in the LO case.

To investigate the origin of the different behaviors and compare in more detail LO and NLO, we perform studies to separate the effects on the fits from (i) NLO corrections to evolution kernels and matrix elements, (ii) two-loop corrections to the running coupling, (iii) small-x and finite-x contributions.[10] The results are reported in the three panels of figure 11.

[10]The inclusion of small-x contributions beyond fixed order into the PB formalism has been explored in [121],

JHEP06(2025)192

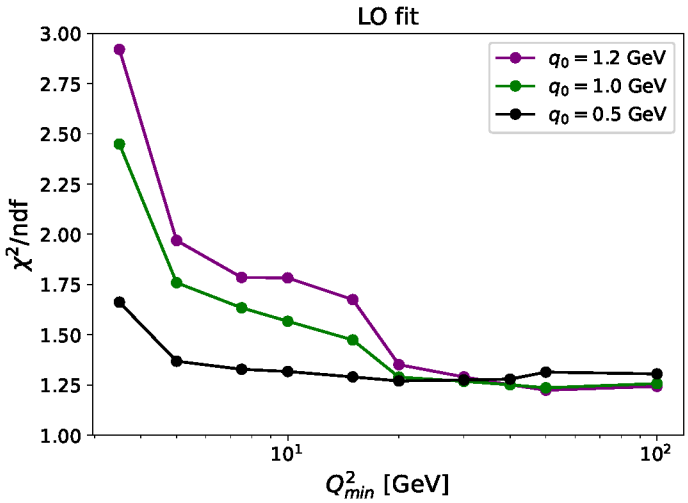

Figure 10. The χ^2/n.d.f. value of the LO dynamical-z_M fit to DIS precision data [62] as a function of the minimum Q^2 of the data included in the fit, for different values of q_0.

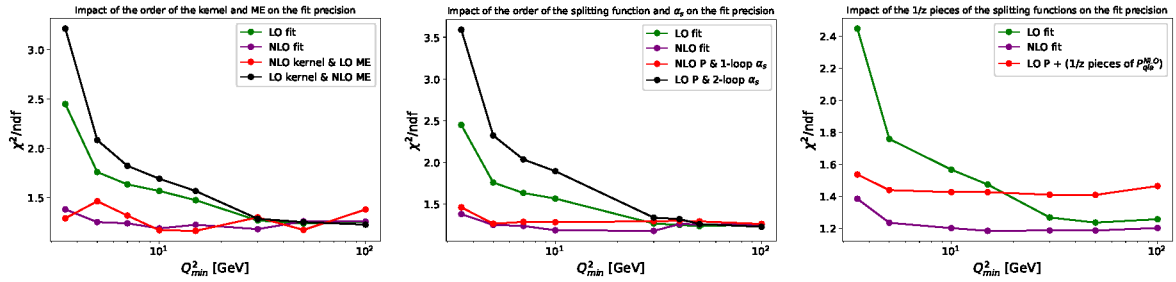

Figure 11. The χ^2/n.d.f. of the $q_0 = 1\,\text{GeV}$ fit versus Q^2_{min} for different scenarios: (left) effect of LO and NLO contributions to evolution kernels and matrix elements; (middle) effect of running coupling and splitting functions to evolution kernels; (right) effect of small-x and finite-x parts of the splitting functions.

All computations in figure 11 are done with $q_0 = 1\,\text{GeV}$. The green and purple curves in each panel are, respectively, the LO and NLO results. In the left panel, these are compared with the black and red curves obtained, respectively, by using LO evolution kernel with NLO matrix element and NLO evolution kernel with LO matrix element. The closeness of the red and purple curves, on one hand, and of the green and black curves, on the other hand, suggests that it is the effect included in the evolution kernel that drives the difference between LO and NLO fits.

The middle panel in figure 11 examines the contributions to the evolution kernel from running coupling and splitting functions. Here, the black and red curves are obtained, respectively, by using LO splitting functions with two-loop running coupling, and NLO splitting functions with one-loop running coupling. The closeness of the red and purple curves, on one hand, and of the green and black curves, on the other hand, suggests that it is the effect included in the splitting functions, rather than α_s, that drives the difference between LO and NLO fits.

using modified CCFM kernels [72, 122, 123], and in [124], using TMD splitting functions [125–130]. We do not include these developments in the present study.

JHEP06(2025)192

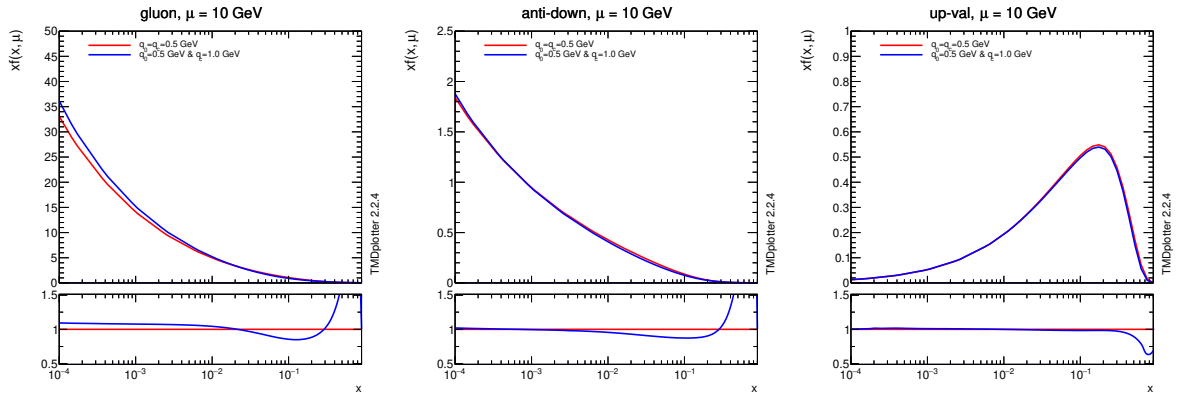

Figure 12. The x dependence of iTMD distributions for different parton species at $\mu = 10\,\text{GeV}$ obtained from the NLO $q_0 = 0.5\,\text{GeV}$ fits with $q_c = 1\,\text{GeV}$ (blue curves) and $q_c = 0.5\,\text{GeV}$ (red curves).

The right panel of figure 11 examines the contributions to the NLO splitting functions from small x and from finite x. Here the red curve is obtained by adding to the LO splitting functions only the $x \to 0$ singular parts of NLO corrections. The behavior of the red curve for small Q^2_{min} is qualitatively similar to the NLO curve, rather than to the LO curve, suggesting that it is the effect included in the small-x parts of the NLO splitting functions that drives the difference between LO and NLO fits, particularly in the region of low Q^2. This result, besides helping to interpret the behavior observed in figures 4, 10, may be useful for studies of small-x dynamics in inclusive-DIS data, e.g. including saturation [131, 132] and resummation [133–139]. As discussed earlier, fits with dynamical z_M at varying q_0 scale, as performed in this paper, probe the impact of the soft Sudakov radiation region; they can provide a useful tool for investigations of Sudakov and small-x effects particularly in low-Q^2 DIS measurements.

3.4 A fit with $q_0 \neq q_c$

As mentioned earlier, while in the fits presented in subsections 3.2 and 3.3 the showering scale q_0 in eq. (2.5) and the scale q_c in the running coupling in eq. (2.6) are set to be equal, the two scales are conceptually distinct, and may be set to different values. In this subsection we present a fit in which $q_0 = 0.5\,\text{GeV}$, $q_c = 1\,\text{GeV}$. This parameter choice may be useful to disentangle the effects from the soft-gluon resolution scale defined by the parameter q_0 and the α_s freezing scale q_c in the pre-confinement picture. In keeping with the notation at the beginning of subsection 3.2, we will name this fit PB-NLO-2025-DynZm-q0-0_5B.

With $q_0 = 0.5\,\text{GeV}$ and $q_c = 1\,\text{GeV}$, we find that the `xFitter` fit converges $\chi^2/n.d.f. = 1.26$.

Figure 12 and figure 13 show, respectively, a comparison of the iTMD and TMD distributions for the sets PB-NLO-2025-DynZm-q0-0_5 and PB-NLO-2025-DynZm-q0-0_5B. The results are similar for most of the kinematic regions and parton channels; however, non-negligible differences arise especially in the gluon distributions and for small transverse momenta.

JHEP06(2025)192

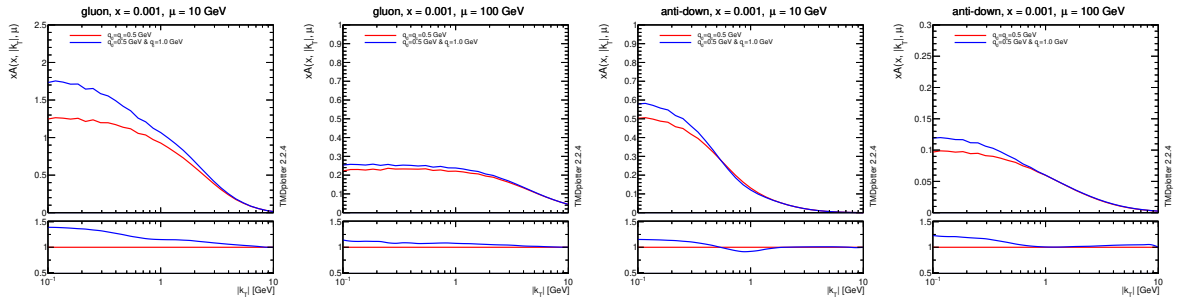

Figure 13. The k_T dependence of TMD distributions for gluon and anti-down quark, at $x = 0.001$ and $\mu = 10$ and 100 GeV, obtained from the NLO $q_0 = 0.5$ GeV fits with $q_c = 1$ GeV (blue curves) and $q_c = 0.5$ GeV (red curves).

4 Application to DY transverse momentum

As an application of the DIS fits with dynamical resolution scale z_M described in section 3, in this section we compute theoretical predictions for the DY transverse momentum distribution, following the method developed in refs. [45, 46], and compare them with experimental data from the LHC and lower-energy experiments. In subsection 4.1 we present the main results, and in subsection 4.2 we give comments and point to further applications.

4.1 PB results with dynamical z_M

For the purpose of this study, we concentrate on the set with $q_0 = 1$ GeV given in section 3. Following the procedure in refs. [45, 46], we first use the integrated TMDs determined in section 3 to generate the DY hard-scattering matrix element at NLO from MCatNLO in the LHE format [140]; we then supplement it with the transverse momentum generated according to the TMD distributions of section 3 by employing the Monte Carlo event generator Cascade3 [66]. The matching of NLO matrix element and PB TMD distributions is performed by using the Herwig6 [141, 142] subtraction term in MCatNLO (a detailed study of the procedure using this subtraction term is performed in the appendix of ref. [143]). Theoretical uncertainties from perturbation theory are estimated within MCatNLO by variation of the renormalization and factorization scale. Besides, uncertainties from the PB TMD distributions as determined in section 3 are included. The events thus generated are analyzed by using the Rivet package [144].

In figure 14 the theoretical predictions thus obtained are compared with 13 TeV CMS data [67]. Similarly to the finding in ref. [45] for the case of fixed z_M, the predictions obtained from PB TMD evolution with NLO matching are capable of describing the data well for low and moderate p_T, while for higher p_T contributions from multiple hard-parton emissions beyond NLO become important and need to be taken into account, as illustrated, e.g., through the TMD multi-jet merging technique in refs. [145–147]. In the present study we focus on the low-p_T region, in which the NLO-matched predictions are sufficient.

Next, we investigate further the predictions obtained with dynamical resolution scale z_M. In particular, we wish to examine the sensitivity of DY measurements to the intrinsic-k_T parameter q_s of the TMD distribution in the dynamical-z_M scenario, by performing a fit of the theoretical predictions to the 13 TeV CMS data [67] for DY transverse momentum. We

JHEP06(2025)192

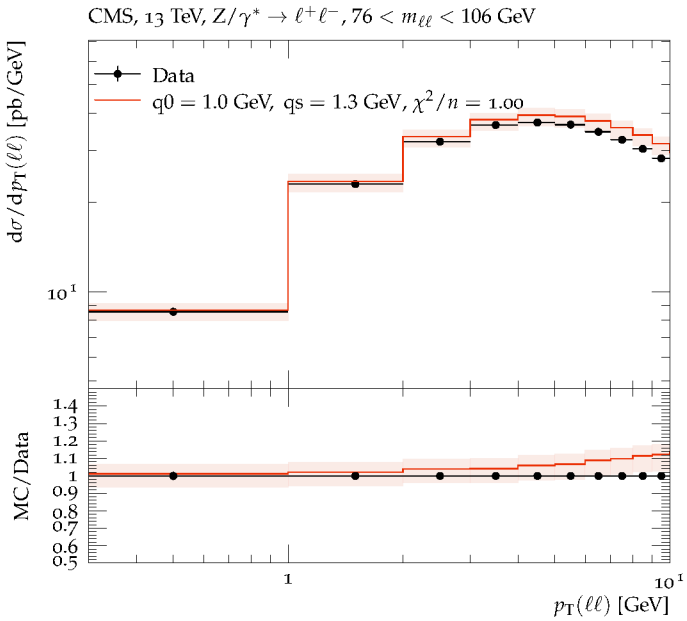

Figure 14. Predictions for the lepton-pair transverse momentum obtained with MCatNLO matched with dynamical-z_M PB TMD distributions with $q_0 = 1$ GeV, compared to 13 TeV CMS data. Uncertainties from perturbative scale variations in MCatNLO are shown.

focus on the DY mass region around the Z-boson peak. We leave a complete intrinsic-k_T analysis, extending to all DY mass regions measured in [67] (from 50 GeV to 1 TeV) and including a full treatment of correlations (as done in ref. [52] for fixed z_M), to future work.

In order to determine the intrinsic k_T that describes the data best, we vary the value of the q_s parameter and for each value we calculate the χ^2 to quantify the model agreement with the measurement. We consider the region of DY transverse momenta $p_T \leq p_{T,\max}$, for different values of $p_{T,\max}$. The results for the χ^2 per degree of freedom versus q_s are shown in figure 15 for the case $p_{T,\max} = 10$ GeV. We have verified the robustness of the result for q_s by varying $p_{T,\max}$ in the range between 5 ad 15 GeV.

The results of the calculation reported in figure 15 indicate that the dynamical-z_M distributions, fitted to precision DIS data in section 3, successfully describe the LHC DY data [67] at low p_T and that sensitivity to the nonperturbative intrinsic-k_T parameter q_s can be achieved from these low-p_T data.

To embed these results in a broader context and further explore the description of DY transverse momentum by predictions with dynamical resolution scale z_M, we turn to DY measurements from lower-energy experiments, and repeat the analysis above in the cases of DY data sets at different energies. Similarly to what is done in refs. [46, 52] for the fixed-z_M scenario, we consider data from the measurements by ATLAS at 8 TeV [94], D0 at 1.8 TeV [96], PHENIX at 200 GeV [99], R209 at 62 GeV [148], NuSea at 38 GeV [149, 150]. In each of these cases, we apply the same method as above, and determine the intrinsic k_T that describes the data best by varying the value of the q_s parameter and computing χ^2 for every value. We find good χ^2 for each of the data sets. The q_s values corresponding to the best χ^2 for each energy are shown in figure 16.

JHEP06(2025)192

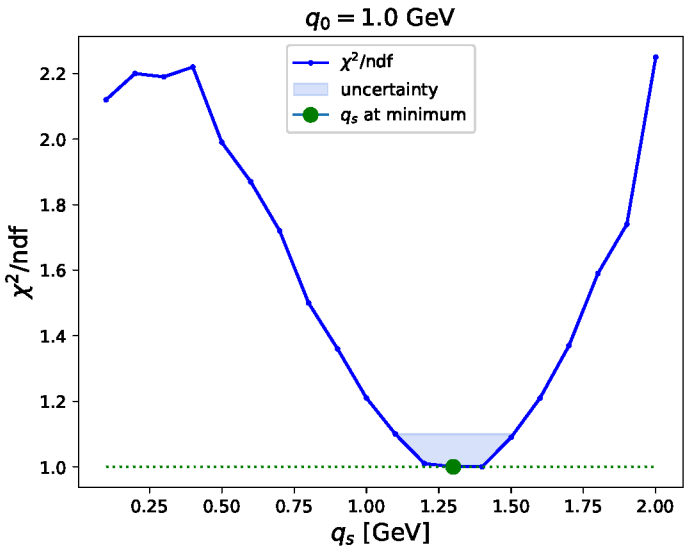

Figure 15. The χ^2/n values versus the q_s parameter from a comparison of the NLO-matched dynamical-z_M predictions at $q_0 = 1.0\,\text{GeV}$ with the CMS measurements [67].

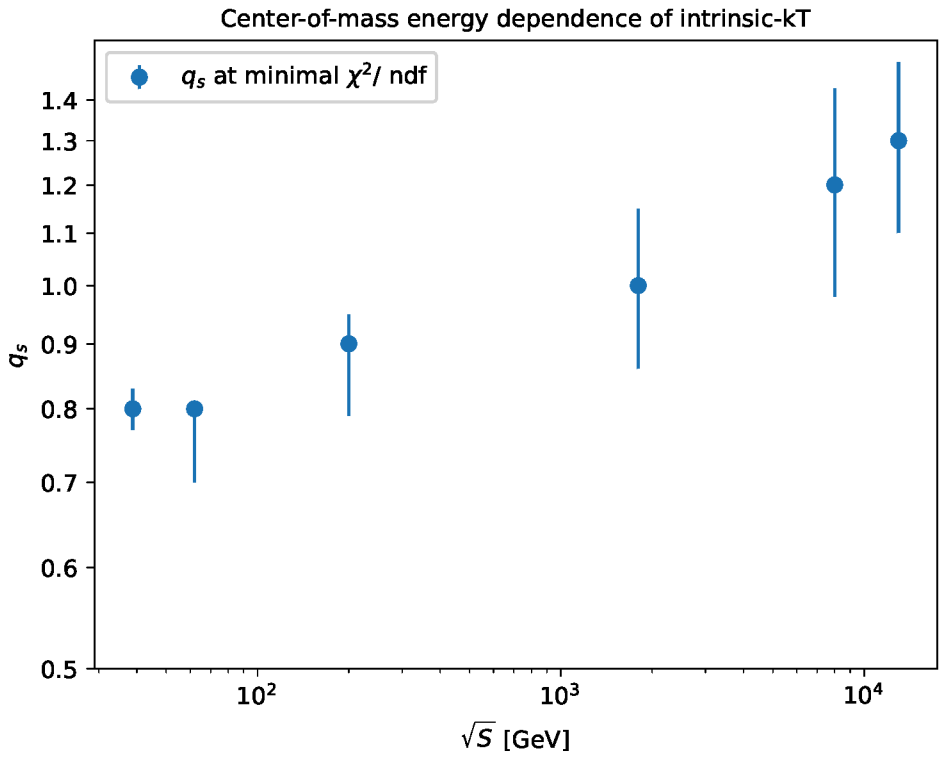

Figure 16. The values of the q_s parameter obtained from a comparison of the NLO-matched dynamical-z_M predictions at $q_0 = 1.0\,\text{GeV}$ with measurements at different energies [67, 94, 96, 99, 148–150].

JHEP06(2025)192

We observe from figure 16 an increase in the value of the intrinsic-k_T parameter q_s with increasing center-of-mass energy. This observation supports the physical picture suggested in ref. [52] and discussed at the end of section 2 in this paper, in which the behavior of the intrinsic k_T is correlated with non-perturbative Sudakov effects near the soft-gluon resolution boundary. In particular, the q_s increase with energy can be associated with dynamical z_M. The results of figure 16 are obtained with showering scale $q_0 = 1\,\text{GeV}$, and suggest that it will be relevant to systematically investigate correlations of q_0 and q_s.

4.2 Comments and future applications

The results of the previous subsection enable further investigations to be carried out in various directions. Since a detailed uncertainty breakdown is available for the measurements [67] and correlations between bins of the measurement are included for each uncertainty source separately, the results of this paper can be extended by carrying out a complete analysis including the full covariance matrix. This can then be compared with the analogous analysis performed, for the fixed-z_M case, in ref. [52] with DY masses from 50 GeV to 1 TeV.

Also, the extraction of q_s from dynamical-z_M fits to DY measurements at different center-of-mass energies, presented in figure 16 for $q_0 = 1\,\text{GeV}$, can be explored further by exploiting the possibility to vary the emissions' minimum transverse momentum q_0 in the soft-gluon resolution z_M. This can help shed light on the transition between the distinct energy behaviors of q_s illustrated by the left hand side panel and right hand side panel in figure 3.

As discussed in section 2, the use of the dynamical resolution scale allows nonperturbative Sudakov contributions to be explored. Ref. [59] presents the PB TMD evaluation of the Collins-Soper kernel as a function of transverse distance b. This is to be compared with recent evaluations of the kernel from lattice calculations [151–164] and from fits to experimental data for transverse momentum spectra [165–168]. In ref. [59], dynamical z_M is found to give rise to a flatter shape in the kernel at large distances b compared to fixed z_M. This behavior is close to the spirit of parton saturation in the s-channel picture [169, 170] for partonic distribution functions, and is phenomenologically relevant since recent fits find that a flat large-b behavior is preferred by data for DY transverse momentum [80] and e^+e^- thrust distribution [171]. An improved understanding of these nonperturbative effects will be important for precision analyses of DY observables involving the lowest measured transverse momenta [172–182].

As a general comment, we note that the analysis of dynamical resolution scales presented in this paper is applicable both to collinear-sensitive observables and to TMD-sensitive observables (in contrast with other approaches which are specifically designed for one or the other class of observables): see e.g. the cases of inclusive DIS structure functions in section 3 and DY transverse momentum distributions in this section. We regard the distributions with dynamical z_M determined in this paper as well-suited to address open issues on the use of parton distributions, both collinear [21, 24, 28, 30] and TMD [29, 108], in parton shower generators.

5 Conclusions

In this work we investigate the role of dynamical soft-gluon resolution scales z_M in PB algorithms, examining parton distributions at both collinear and TMD level.

JHEP06(2025)192

At collinear level, the motivation for this study comes from the potential systematic mismatch arising in parton shower Monte Carlo event generators due to the fact that the resolution scale is used in the shower evolution but not in the PDF evolution. At TMD level, the motivation comes from the interplay of the resolution scale with the transverse momentum recoils in the shower, and possibly with the non-perturbative intrinsic transverse momentum.

The main result of this work is that we obtain a set of collinear and TMD parton distributions from fits to precision DIS data performed by using PDF and TMD evolution with dynamical z_M, as in parton showers. This is done working at NLO in perturbation theory. The dynamical-z_M set includes experimental and model uncertainties. We show that this set not only gives a good fit to precision DIS data but also is capable of describing DY transverse momentum data.

To illustrate this quantitatively, we perform a fit to DY transverse momentum measurements at the LHC and carry out the extraction of the non-perturbative TMD parameter q_s, representing the intrinsic transverse momentum, for the first time in the presence of dynamical resolution scales. We further perform fits to DY transverse momentum measurements from lower-energy experiments at Tevatron, RHIC and fixed target, extract q_s and present its energy dependence.

We expect the results of this paper to be useful for several applications. The collinear distributions with dynamical z_M can be applied to explore open issues on the use of PDFs in parton shower generators. The TMD distributions with dynamical z_M can be applied to investigate non-perturbative Sudakov contributions, and address open questions on the energy dependence as well as mass dependence of intrinsic transverse momentum.

Acknowledgments

We thank H. Jung for useful discussions. A. Lelek acknowledges funding by Research Foundation-Flanders (FWO) (applications' numbers: 1272421N, 1278325N). S. Sadeghi Barzani acknowledges funding by the University of Antwerp Research Fund (BOF). S. Taheri Monfared acknowledges the support of the German Research Foundation (DFG) under grant number 467467041.

Data Availability Statement. This article has no associated data or the data will not be deposited.

Code Availability Statement. This article has no associated code or the code will not be deposited.

JHEP06(2025)192

References

[1] P. Azzi et al., *Report from Working Group 1: Standard Model Physics at the HL-LHC and HE-LHC*, *CERN Yellow Rep. Monogr.* **7** (2019) 1 [arXiv:1902.04070] [INSPIRE].

[2] LHeC and FCC-he Study Group collaborations, *The Large Hadron–Electron Collider at the HL-LHC*, *J. Phys. G* **48** (2021) 110501 [arXiv:2007.14491] [INSPIRE].

[3] FCC collaboration, *FCC Physics Opportunities: Future Circular Collider Conceptual Design Report Volume 1*, *Eur. Phys. J. C* **79** (2019) 474 [INSPIRE].

[4] Y. Hatta et al., *Proceedings, Probing Nucleons and Nuclei in High Energy Collisions: dedicated to the Physics of the Electron Ion Collider: Seattle (WA), United States, October 1 - November 16, 2018*, WSP (2020) [DOI:10.1142/11684] [INSPIRE].

[5] CEPC Physics Study Group collaboration, *The physics potential of the CEPC. Prepared for the US Snowmass Community Planning Exercise (Snowmass 2021)*, in the proceedings of the *Snowmass 2021*, Seattle, U.S.A., July 17–26 (2022) [arXiv:2205.08553] [INSPIRE].

[6] S. Alioli et al., *Monte Carlo event generators for high energy particle physics event simulation*, arXiv:1902.01674 [INSPIRE].

[7] H.-U. Bengtsson and T. Sjostrand, *The Lund Monte Carlo for Hadronic Processes: Pythia Version 4.8*, *Comput. Phys. Commun.* **46** (1987) 43 [INSPIRE].

[8] G. Marchesini and B.R. Webber, *Monte Carlo Simulation of General Hard Processes with Coherent QCD Radiation*, *Nucl. Phys. B* **310** (1988) 461 [INSPIRE].

[9] V.N. Gribov and L.N. Lipatov, *Deep inelastic e p scattering in perturbation theory*, *Sov. J. Nucl. Phys.* **15** (1972) 438 [INSPIRE].

[10] G. Altarelli and G. Parisi, *Asymptotic Freedom in Parton Language*, *Nucl. Phys. B* **126** (1977) 298 [INSPIRE].

[11] Y.L. Dokshitzer, *Calculation of the Structure Functions for Deep Inelastic Scattering and e^+e^- Annihilation by Perturbation Theory in Quantum Chromodynamics*, *Sov. Phys. JETP* **46** (1977) 641 [INSPIRE].

[12] S. Jadach and M. Skrzypek, *Exact solutions of the QCD evolution equations using Monte Carlo method*, *Acta Phys. Polon. B* **35** (2004) 745 [hep-ph/0312355] [INSPIRE].

[13] H. Tanaka, *Initial state parton evolution beyond the leading logarithmic order of QCD*, *Prog. Theor. Phys.* **110** (2003) 963 [INSPIRE].

[14] Y. Kurihara et al., *QCD event generators with next-to-leading order matrix elements and parton showers*, *Nucl. Phys. B* **654** (2003) 301 [hep-ph/0212216] [INSPIRE].

[15] H. Tanaka, T. Sugiura and Y. Wakabayashi, *Factorization algorithm for parton showers beyond the leading logarithmic order of QCD*, *Prog. Theor. Phys.* **114** (2005) 477 [hep-ph/0510185] [INSPIRE].

[16] K.J. Golec-Biernat, S. Jadach, W. Placzek and M. Skrzypek, *Markovian Monte Carlo solutions of the NLO QCD evolution equations*, *Acta Phys. Polon. B* **37** (2006) 1785 [hep-ph/0603031] [INSPIRE].

[17] S. Jadach, M. Skrzypek, A. Kusina and M. Slawinska, *Exclusive Monte Carlo Modelling of NLO DGLAP Evolution*, *PoS* **RADCOR2009** (2010) 069 [arXiv:1002.0010] [INSPIRE].

[18] A. Kusina, S. Jadach, M. Skrzypek and M. Slawinska, *Properties of Inclusive Versus Exclusive QCD Evolution Kernels*, *Acta Phys. Polon. B* **41** (2010) 1683 [arXiv:1004.4131] [INSPIRE].

JHEP06(2025)192

[19] S. Jadach et al., *NLO corrections to hard process in QCD shower — proof of concept*, *Acta Phys. Polon. B* **43** (2012) 2067 [arXiv:1209.4291] [INSPIRE].

[20] Z. Nagy and D.E. Soper, *Parton distribution functions in the context of parton showers*, *JHEP* **06** (2014) 179 [arXiv:1401.6368] [INSPIRE].

[21] Z. Nagy and D.E. Soper, *Evolution of parton showers and parton distribution functions*, *Phys. Rev. D* **102** (2020) 014025 [arXiv:2002.04125] [INSPIRE].

[22] F. Hautmann et al., *Soft-gluon resolution scale in QCD evolution equations*, *Phys. Lett. B* **772** (2017) 446 [arXiv:1704.01757] [INSPIRE].

[23] S. Höche, F. Krauss and S. Prestel, *Implementing NLO DGLAP evolution in Parton Showers*, *JHEP* **10** (2017) 093 [arXiv:1705.00982] [INSPIRE].

[24] S. Amoroso et al., *Les Houches 2019: Physics at TeV Colliders: Standard Model Working Group Report*, in the proceedings of the *11th Les Houches Workshop on Physics at TeV Colliders: PhysTeV Les Houches*, Les Houches, France, June 10–28 (2019) [arXiv:2003.01700] [INSPIRE].

[25] M. van Beekveld and S. Ferrario Ravasio, *Next-to-leading-logarithmic PanScales showers for Deep Inelastic Scattering and Vector Boson Fusion*, *JHEP* **02** (2024) 001 [arXiv:2305.08645] [INSPIRE].

[26] M. van Beekveld et al., *PanScales showers for hadron collisions: all-order validation*, *JHEP* **11** (2022) 020 [arXiv:2207.09467] [INSPIRE].

[27] M. van Beekveld et al., *PanScales parton showers for hadron collisions: formulation and fixed-order studies*, *JHEP* **11** (2022) 019 [arXiv:2205.02237] [INSPIRE].

[28] M. Mendizabal, F. Guzman, H. Jung and S. Taheri Monfared, *On the role of soft and non-perturbative gluons in collinear parton densities and parton shower event generators*, *Eur. Phys. J. C* **84** (2024) 1299 [arXiv:2309.11802] [INSPIRE].

[29] H. Jung, *The non-perturbative Sudakov Form Factor and the role of soft gluons*, in the proceedings of the *30th Cracow Epiphany Conference on on Precision Physics at High Energy Colliders: dedicated to the memory of Staszek Jadach*, Cracow, Poland, January 08–12 (2024) [arXiv:2404.06905] [INSPIRE].

[30] S. Frixione and B.R. Webber, *Correcting for cutoff dependence in backward evolution of QCD parton showers*, *JHEP* **03** (2024) 150 [arXiv:2309.15587] [INSPIRE].

[31] H. Jung, L. Lönnblad, M. Mendizabal and S. Taheri Monfared, *A parton shower consistent with parton densities at LO and NLO: PDF2ISR*, arXiv:2504.10243 [INSPIRE].

[32] J. Bellm et al., *Herwig 7.0/Herwig++ 3.0 release note*, *Eur. Phys. J. C* **76** (2016) 196 [arXiv:1512.01178] [INSPIRE].

[33] M. Bahr et al., *Herwig++ Physics and Manual*, *Eur. Phys. J. C* **58** (2008) 639 [arXiv:0803.0883] [INSPIRE].

[34] C. Bierlich et al., *A comprehensive guide to the physics and usage of PYTHIA 8.3*, *SciPost Phys. Codeb.* **2022** (2022) 8 [arXiv:2203.11601] [INSPIRE].

[35] T. Sjöstrand et al., *An introduction to PYTHIA 8.2*, *Comput. Phys. Commun.* **191** (2015) 159 [arXiv:1410.3012] [INSPIRE].

[36] SHERPA collaboration, *Event Generation with Sherpa 2.2*, *SciPost Phys.* **7** (2019) 034 [arXiv:1905.09127] [INSPIRE].

[37] T. Gleisberg et al., *Event generation with SHERPA 1.1*, *JHEP* **02** (2009) 007 [arXiv:0811.4622] [INSPIRE].

JHEP06(2025)192

[38] S. Dooling, P. Gunnellini, F. Hautmann and H. Jung, *Longitudinal momentum shifts, showering, and nonperturbative corrections in matched next-to-leading-order shower event generators*, *Phys. Rev. D* **87** (2013) 094009 [arXiv:1212.6164] [INSPIRE].

[39] F. Hautmann and H. Jung, *Collinearity approximations and kinematic shifts in partonic shower algorithms*, *Eur. Phys. J. C* **72** (2012) 2254 [arXiv:1209.6549] [INSPIRE].

[40] R. Angeles-Martinez et al., *Transverse Momentum Dependent (TMD) parton distribution functions: status and prospects*, *Acta Phys. Polon. B* **46** (2015) 2501 [arXiv:1507.05267] [INSPIRE].

[41] T.C. Rogers, *An overview of transverse-momentum-dependent factorization and evolution*, *Eur. Phys. J. A* **52** (2016) 153 [arXiv:1509.04766] [INSPIRE].

[42] R. Boussarie et al., *TMD Handbook*, arXiv:2304.03302 [INSPIRE].

[43] F. Hautmann et al., *Collinear and TMD Quark and Gluon Densities from Parton Branching Solution of QCD Evolution Equations*, *JHEP* **01** (2018) 070 [arXiv:1708.03279] [INSPIRE].

[44] A. Bermudez Martinez et al., *Collinear and TMD parton densities from fits to precision DIS measurements in the parton branching method*, *Phys. Rev. D* **99** (2019) 074008 [arXiv:1804.11152] [INSPIRE].

[45] A. Bermudez Martinez et al., *Production of Z-bosons in the parton branching method*, *Phys. Rev. D* **100** (2019) 074027 [arXiv:1906.00919] [INSPIRE].

[46] A. Bermudez Martinez et al., *The transverse momentum spectrum of low mass Drell-Yan production at next-to-leading order in the parton branching method*, *Eur. Phys. J. C* **80** (2020) 598 [arXiv:2001.06488] [INSPIRE].

[47] M.I. Abdulhamid et al., *Azimuthal correlations of high transverse momentum jets at next-to-leading order in the parton branching method*, *Eur. Phys. J. C* **82** (2022) 36 [arXiv:2112.10465] [INSPIRE].

[48] A. Bermudez Martinez and F. Hautmann, *Azimuthal di-jet correlations with parton branching TMD distributions*, in the proceedings of the *29th International Workshop on Deep-Inelastic Scattering and Related Subjects*, Santiago de Compostela, Spain, May 02–06 (2022) [arXiv:2208.08446] [INSPIRE].

[49] F. Hautmann, L. Keersmaekers, A. Lelek and A.M. Van Kampen, *Dynamical resolution scale in transverse momentum distributions at the LHC*, *Nucl. Phys. B* **949** (2019) 114795 [arXiv:1908.08524] [INSPIRE].

[50] S. Catani, B.R. Webber and G. Marchesini, *QCD coherent branching and semiinclusive processes at large x*, *Nucl. Phys. B* **349** (1991) 635 [INSPIRE].

[51] B.R. Webber, *Monte Carlo Simulation of Hard Hadronic Processes*, *Ann. Rev. Nucl. Part. Sci.* **36** (1986) 253 [INSPIRE].

[52] I. Bubanja et al., *The small $k_T$region in Drell-Yan production at next-to-leading order with the parton branching method*, *Eur. Phys. J. C* **84** (2024) 154 [arXiv:2312.08655] [INSPIRE].

[53] CMS collaboration, *Energy-scaling behavior of intrinsic transverse-momentum parameters in Drell-Yan simulation*, *Phys. Rev. D* **111** (2025) 072003 [arXiv:2409.17770] [INSPIRE].

[54] CMS collaboration, *Energy scaling behavior of intrinsic transverse momentum in Drell-Yan events*, CMS-PAS-GEN-22-001, CERN, Geneva (2024).

[55] CMS collaboration, *Extraction and validation of a new set of CMS PYTHIA8 tunes from underlying-event measurements*, *Eur. Phys. J. C* **80** (2020) 4 [arXiv:1903.12179] [INSPIRE].

JHEP06(2025)192

[56] P. Skands, S. Carrazza and J. Rojo, *Tuning PYTHIA 8.1: the Monash 2013 Tune*, *Eur. Phys. J. C* **74** (2014) 3024 [arXiv:1404.5630] [INSPIRE].

[57] CMS collaboration, *Development and validation of HERWIG 7 tunes from CMS underlying-event measurements*, *Eur. Phys. J. C* **81** (2021) 312 [arXiv:2011.03422] [INSPIRE].

[58] A. Buckley et al., *Systematic event generator tuning for the LHC*, *Eur. Phys. J. C* **65** (2010) 331 [arXiv:0907.2973] [INSPIRE].

[59] A.B. Martinez et al., *Soft-gluon coupling and the TMD parton branching Sudakov form factor*, arXiv:2412.21116 [INSPIRE].

[60] A.B. Martinez et al., *The Parton Branching Sudakov and its relation to CSS*, *PoS* **EPS-HEP2023** (2024) 270 [INSPIRE].

[61] A. Lelek, *NNLL Transverse Momentum Dependent evolution in the Parton Branching method*, in the proceedings of the *42nd International Symposium on Physics In Collision*, Arica, Chile, October 10–13 (2023) [arXiv:2412.09108] [INSPIRE].

[62] H1 and ZEUS collaborations, *Combination of measurements of inclusive deep inelastic $e^{\pm}p$ scattering cross sections and QCD analysis of HERA data*, *Eur. Phys. J. C* **75** (2015) 580 [arXiv:1506.06042] [INSPIRE].

[63] xFITTER collaboration, *xFitter: an Open Source QCD Analysis Framework. A resource and reference document for the Snowmass study*, arXiv:2206.12465 [INSPIRE].

[64] S. Alekhin et al., *HERAFitter*, *Eur. Phys. J. C* **75** (2015) 304 [arXiv:1410.4412] [INSPIRE].

[65] J. Alwall et al., *The automated computation of tree-level and next-to-leading order differential cross sections, and their matching to parton shower simulations*, *JHEP* **07** (2014) 079 [arXiv:1405.0301] [INSPIRE].

[66] CASCADE collaboration, *CASCADE3 A Monte Carlo event generator based on TMDs*, *Eur. Phys. J. C* **81** (2021) 425 [arXiv:2101.10221] [INSPIRE].

[67] CMS collaboration, *Measurement of the mass dependence of the transverse momentum of lepton pairs in Drell-Yan production in proton-proton collisions at $\sqrt{s} = 13$ TeV*, *Eur. Phys. J. C* **83** (2023) 628 [arXiv:2205.04897] [INSPIRE].

[68] H1 collaboration, *Measurement of the 1-jettiness event shape observable in deep-inelastic electron-proton scattering at HERA*, *Eur. Phys. J. C* **84** (2024) 785 [arXiv:2403.10109] [INSPIRE].

[69] H1 collaboration, *Measurement of Lepton-Jet Correlation in Deep-Inelastic Scattering with the H1 Detector Using Machine Learning for Unfolding*, *Phys. Rev. Lett.* **128** (2022) 132002 [arXiv:2108.12376] [INSPIRE].

[70] A. Banfi et al., *A POWHEG generator for deep inelastic scattering*, *JHEP* **02** (2024) 023 [arXiv:2309.02127] [INSPIRE].

[71] CASCADE collaboration, *The CCFM Monte Carlo generator CASCADE version 2.2.03*, *Eur. Phys. J. C* **70** (2010) 1237 [arXiv:1008.0152] [INSPIRE].

[72] F. Hautmann and H. Jung, *Angular correlations in multi-jet final states from k-perpendicular - dependent parton showers*, *JHEP* **10** (2008) 113 [arXiv:0805.1049] [INSPIRE].

[73] F. Hautmann and H. Jung, *Three-jet DIS final states from k(T)-dependent parton showers*, *PoS* **RADCOR2007** (2007) 030 [arXiv:0804.1746] [INSPIRE].

[74] Y.L. Dokshitzer, V.A. Khoze, S.I. Troian and A.H. Mueller, *QCD Coherence in High-Energy Reactions*, *Rev. Mod. Phys.* **60** (1988) 373 [INSPIRE].

JHEP06(2025)192

[75] A. Bassetto, M. Ciafaloni and G. Marchesini, *Jet Structure and Infrared Sensitive Quantities in Perturbative QCD*, *Phys. Rept.* **100** (1983) 201 [INSPIRE].

[76] D. Amati et al., *A Treatment of Hard Processes Sensitive to the Infrared Structure of QCD*, *Nucl. Phys. B* **173** (1980) 429 [INSPIRE].

[77] J.C. Collins, D.E. Soper and G.F. Sterman, *Transverse Momentum Distribution in Drell-Yan Pair and W and Z Boson Production*, *Nucl. Phys. B* **250** (1985) 199 [INSPIRE].

[78] J. Collins, *Foundations of Perturbative QCD*, Cambridge University Press (2011) [DOI:10.1017/9781009401845] [INSPIRE].

[79] I. Scimemi and A. Vladimirov, *Systematic analysis of double-scale evolution*, *JHEP* **08** (2018) 003 [arXiv:1803.11089] [INSPIRE].

[80] F. Hautmann, I. Scimemi and A. Vladimirov, *Non-perturbative contributions to vector-boson transverse momentum spectra in hadronic collisions*, *Phys. Lett. B* **806** (2020) 135478 [arXiv:2002.12810] [INSPIRE].

[81] F. Hautmann, *Endpoint singularities in unintegrated parton distributions*, *Phys. Lett. B* **655** (2007) 26 [hep-ph/0702196] [INSPIRE].

[82] F. Hautmann, I. Scimemi and A. Vladimirov, *Determination of the rapidity evolution kernel from Drell-Yan data at low transverse momenta*, *SciPost Phys. Proc.* **8** (2022) 123 [arXiv:2109.12051] [INSPIRE].

[83] J.C. Collins and D.E. Soper, *Back-To-Back Jets in QCD*, *Nucl. Phys. B* **193** (1981) 381 [*Erratum ibid.* **213** (1983) 545] [INSPIRE].

[84] J.C. Collins and D.E. Soper, *Back-To-Back Jets: Fourier Transform from B to K-Transverse*, *Nucl. Phys. B* **197** (1982) 446 [INSPIRE].

[85] M.A. Kimber, A.D. Martin and M.G. Ryskin, *Unintegrated parton distributions and prompt photon hadroproduction*, *Eur. Phys. J. C* **12** (2000) 655 [hep-ph/9911379] [INSPIRE].

[86] A.D. Martin, M.G. Ryskin and G. Watt, *NLO prescription for unintegrated parton distributions*, *Eur. Phys. J. C* **66** (2010) 163 [arXiv:0909.5529] [INSPIRE].

[87] B. Guiot and A. van Hameren, *Examination of k_t-factorization in a Yukawa theory*, *JHEP* **04** (2024) 085 [arXiv:2401.06888] [INSPIRE].

[88] F. Aslan et al., *Basics of factorization in a scalar Yukawa field theory*, *Phys. Rev. D* **107** (2023) 074031 [arXiv:2212.00757] [INSPIRE].

[89] B. Guiot, *Normalization of unintegrated parton densities*, *Phys. Rev. D* **107** (2023) 014015 [*Erratum ibid.* **110** (2024) 039901] [arXiv:2205.02873] [INSPIRE].

[90] M.A. Nefedov and V.A. Saleev, *High-Energy Factorization for Drell-Yan process in pp and $p\bar{p}$ collisions with new Unintegrated PDFs*, *Phys. Rev. D* **102** (2020) 114018 [arXiv:2009.13188] [INSPIRE].

[91] B. Guiot, *Pathologies of the Kimber-Martin-Ryskin prescriptions for unintegrated PDFs: which prescription should be preferred?*, *Phys. Rev. D* **101** (2020) 054006 [arXiv:1910.09656] [INSPIRE].

[92] K. Golec-Biernat and A.M. Stasto, *On the use of the KMR unintegrated parton distribution functions*, *Phys. Lett. B* **781** (2018) 633 [arXiv:1803.06246] [INSPIRE].

[93] W. Zhan et al., *Coarse-grained binning in Drell-Yan transverse momentum spectra*, *Phys. Rev. D* **111** (2025) 036018 [arXiv:2412.19060] [INSPIRE].

JHEP06(2025)192

[94] ATLAS collaboration, *Measurement of the transverse momentum and ϕ^*_η distributions of Drell-Yan lepton pairs in proton–proton collisions at $\sqrt{s} = 8$ TeV with the ATLAS detector*, *Eur. Phys. J. C* **76** (2016) 291 [arXiv:1512.02192] [INSPIRE].

[95] LHCb collaboration, *Precision measurement of forward Z boson production in proton-proton collisions at $\sqrt{s} = 13$ TeV*, *JHEP* **07** (2022) 026 [arXiv:2112.07458] [INSPIRE].

[96] D0 collaboration, *Measurement of the inclusive differential cross section for Z bosons as a function of transverse momentum in $\bar{p}p$ collisions at $\sqrt{s} = 1.8$ TeV*, *Phys. Rev. D* **61** (2000) 032004 [hep-ex/9907009] [INSPIRE].

[97] CDF collaboration, *The transverse momentum and total cross section of e^+e^- pairs in the Z boson region from $p\bar{p}$ collisions at $\sqrt{s} = 1.8$ TeV*, *Phys. Rev. Lett.* **84** (2000) 845 [hep-ex/0001021] [INSPIRE].

[98] CDF collaboration, *Transverse momentum cross section of e^+e^- pairs in the Z-boson region from $p\bar{p}$ collisions at $\sqrt{s} = 1.96$ TeV*, *Phys. Rev. D* **86** (2012) 052010 [arXiv:1207.7138] [INSPIRE].

[99] PHENIX collaboration, *Measurements of $\mu\mu$ pairs from open heavy flavor and Drell-Yan in $p + p$ collisions at $\sqrt{s} = 200$ GeV*, *Phys. Rev. D* **99** (2019) 072003 [arXiv:1805.02448] [INSPIRE].

[100] CMS collaboration, *Study of Drell-Yan dimuon production in proton-lead collisions at $\sqrt{s_{\rm NN}} = 8.16$ TeV*, *JHEP* **05** (2021) 182 [arXiv:2102.13648] [INSPIRE].

[101] G. Moreno et al., *Dimuon Production in Proton–Copper Collisions at $\sqrt{s} = 38.8$-GeV*, *Phys. Rev. D* **43** (1991) 2815 [INSPIRE].

[102] W. Zhan et al., *A p_T-ratio observable for studies of intrinsic transverse momentum of partons from Drell-Yan p_T spectra*, in the proceedings of the *59th Rencontres de Moriond on QCD and High Energy Interactions: Moriond QCD 2025*, La Thuille, Italy, March 30 – April 06 (2025) [arXiv:2505.06973] [INSPIRE].

[103] S. Gieseke, M.H. Seymour and A. Siodmok, *A model of non-perturbative gluon emission in an initial state parton shower*, *JHEP* **06** (2008) 001 [arXiv:0712.1199] [INSPIRE].

[104] T. Sjostrand and P.Z. Skands, *Multiple interactions and the structure of beam remnants*, *JHEP* **03** (2004) 053 [hep-ph/0402078] [INSPIRE].

[105] I. Bubanja et al., *Center-of-mass energy dependence of intrinsic-k_T distributions obtained from Drell-Yan production*, *Eur. Phys. J. C* **85** (2025) 278 [arXiv:2404.04088] [INSPIRE].

[106] I. Bubanja, H. Jung, N. Raicevic and S. Taheri Monfared, *Interplay of intrinsic motion of partons and soft gluon emissions in Drell-Yan production studied with PYTHIA*, *Eur. Phys. J. C* **85** (2025) 363 [arXiv:2412.05221] [INSPIRE].

[107] N. Raicevic, *The role of the Intrinsic-k_T and Soft Gluon Contributions in Drell-Yan Production*, *Phys. Part. Nucl. Lett.* **22** (2025) 156 [arXiv:2408.11013] [INSPIRE].

[108] CASCADE collaboration, *Non-perturbative contributions to low transverse momentum Drell-Yan pair production using the Parton Branching Method*, *Phys. Scripta* **100** (2025) 045306 [arXiv:2412.00892] [INSPIRE].

[109] S. Taheri Monfared, *Recent Progress in Transverse Momentum-Dependent Parton Densities and Corresponding Parton Showers*, *PoS* **DIS2024** (2025) 041 [arXiv:2410.05853] [INSPIRE].

[110] S. Taheri Monfared, *What can we learn from the Parton Branching method in QCD?*, arXiv:2412.14037 [INSPIRE].

JHEP06(2025)192

[111] S.S. Barzani, *PB TMD fits at NLO with dynamical resolution scale*, in the proceedings of the *29th International Workshop on Deep-Inelastic Scattering and Related Subjects*, Santiago de Compostela, Spain, May 02–06 (2022) [arXiv:2207.13519] [INSPIRE].

[112] N.A. Abdulov et al., *TMDlib2 and TMDplotter: a platform for 3D hadron structure studies*, *Eur. Phys. J. C* **81** (2021) 752 [arXiv:2103.09741] [INSPIRE].

[113] F. Hautmann et al., *TMDlib and TMDplotter: library and plotting tools for transverse-momentum-dependent parton distributions*, *Eur. Phys. J. C* **74** (2014) 3220 [arXiv:1408.3015] [INSPIRE].

[114] F. Hautmann and H. Jung, *Transverse momentum dependent gluon density from DIS precision data*, *Nucl. Phys. B* **883** (2014) 1 [arXiv:1312.7875] [INSPIRE].

[115] H. Jung and F. Hautmann, *Determination of transverse momentum dependent gluon density from HERA structure function measurements*, in the proceedings of the *20th International Workshop on Deep-Inelastic Scattering and Related Subjects*, Bonn, Germany, March 26–30 (2012) [DOI:10.3204/DESY-PROC-2012-02/29] [arXiv:1206.1796] [INSPIRE].

[116] F. Hautmann, H. Jung and S.T. Monfared, *The CCFM uPDF evolution uPDFevolv Version 1.0.00*, *Eur. Phys. J. C* **74** (2014) 3082 [arXiv:1407.5935] [INSPIRE].

[117] H. Jung, A. Lelek, K.M. Figueroa and S. Taheri Monfared, *The Parton Branching evolution package uPDFevolv2*, arXiv:2405.20185 [INSPIRE].

[118] J. Pumplin et al., *Uncertainties of predictions from parton distribution functions. 2. The Hessian method*, *Phys. Rev. D* **65** (2001) 014013 [hep-ph/0101032] [INSPIRE].

[119] H1 and ZEUS collaborations, *Combination and QCD analysis of charm and beauty production cross-section measurements in deep inelastic ep scattering at HERA*, *Eur. Phys. J. C* **78** (2018) 473 [arXiv:1804.01019] [INSPIRE].

[120] H1 and ZEUS collaborations, *Combination and QCD Analysis of Charm Production Cross Section Measurements in Deep-Inelastic ep Scattering at HERA*, *Eur. Phys. J. C* **73** (2013) 2311 [arXiv:1211.1182] [INSPIRE].

[121] S. Taheri Monfared, F. Hautmann, H. Jung and M. Schmitz, *Extending parton branching TMDs to small x*, *PoS* **DIS2019** (2019) 136 [arXiv:1908.01621] [INSPIRE].

[122] S. Catani, F. Fiorani and G. Marchesini, *Small x Behavior of Initial State Radiation in Perturbative QCD*, *Nucl. Phys. B* **336** (1990) 18 [INSPIRE].

[123] M. Ciafaloni, *Coherence Effects in Initial Jets at Small q**2 / s*, *Nucl. Phys. B* **296** (1988) 49 [INSPIRE].

[124] F. Hautmann et al., *A parton branching with transverse momentum dependent splitting functions*, *Phys. Lett. B* **833** (2022) 137276 [arXiv:2205.15873] [INSPIRE].

[125] S. Catani and F. Hautmann, *Quark anomalous dimensions at small x*, *Phys. Lett. B* **315** (1993) 157 [INSPIRE].

[126] S. Catani and F. Hautmann, *High-energy factorization and small x deep inelastic scattering beyond leading order*, *Nucl. Phys. B* **427** (1994) 475 [hep-ph/9405388] [INSPIRE].

[127] F. Hautmann, M. Hentschinski and H. Jung, *Forward Z-boson production and the unintegrated sea quark density*, *Nucl. Phys. B* **865** (2012) 54 [arXiv:1205.1759] [INSPIRE].

[128] O. Gituliar, M. Hentschinski and K. Kutak, *Transverse-momentum-dependent quark splitting functions in k_T-factorization: real contributions*, *JHEP* **01** (2016) 181 [arXiv:1511.08439] [INSPIRE].

JHEP06(2025)192

[129] M. Hentschinski, A. Kusina and K. Kutak, *Transverse momentum dependent splitting functions at work: quark-to-gluon splitting*, *Phys. Rev. D* **94** (2016) 114013 [arXiv:1607.01507] [INSPIRE].

[130] M. Hentschinski, A. Kusina, K. Kutak and M. Serino, *TMD splitting functions in k_T factorization: the real contribution to the gluon-to-gluon splitting*, *Eur. Phys. J. C* **78** (2018) 174 [arXiv:1711.04587] [INSPIRE].

[131] N. Armesto et al., *Signatures of gluon saturation from structure-function measurements*, *Phys. Rev. D* **105** (2022) 114017 [arXiv:2203.05846] [INSPIRE].

[132] G. Beuf, H. Hänninen, T. Lappi and H. Mäntysaari, *Color Glass Condensate at next-to-leading order meets HERA data*, *Phys. Rev. D* **102** (2020) 074028 [arXiv:2007.01645] [INSPIRE].

[133] xFitter Developers' Team collaboration, *Impact of low-x resummation on QCD analysis of HERA data*, *Eur. Phys. J. C* **78** (2018) 621 [arXiv:1802.00064] [INSPIRE].

[134] R.D. Ball et al., *Parton distributions with small-x resummation: evidence for BFKL dynamics in HERA data*, *Eur. Phys. J. C* **78** (2018) 321 [arXiv:1710.05935] [INSPIRE].

[135] G. Altarelli, R.D. Ball and S. Forte, *Small x Resummation with Quarks: Deep-Inelastic Scattering*, *Nucl. Phys. B* **799** (2008) 199 [arXiv:0802.0032] [INSPIRE].

[136] R.K. Ellis, F. Hautmann and B.R. Webber, *QCD scaling violation at small x*, *Phys. Lett. B* **348** (1995) 582 [hep-ph/9501307] [INSPIRE].

[137] M. Ciafaloni, D. Colferai, G.P. Salam and A.M. Stasto, *A matrix formulation for small-x singlet evolution*, *JHEP* **08** (2007) 046 [arXiv:0707.1453] [INSPIRE].

[138] A.V. Lipatov, G.I. Lykasov and M.A. Malyshev, *Refined TMD Gluon Density in a Proton from the HERA and LHC Data*, *JETP Lett.* **119** (2024) 828 [arXiv:2404.09550] [INSPIRE].

[139] C.D. White and R.S. Thorne, *A Global Fit to Scattering Data with NLL BFKL Resummations*, *Phys. Rev. D* **75** (2007) 034005 [hep-ph/0611204] [INSPIRE].

[140] J. Alwall et al., *A standard format for Les Houches event files*, *Comput. Phys. Commun.* **176** (2007) 300 [hep-ph/0609017] [INSPIRE].

[141] G. Corcella et al., *HERWIG 6.5 release note*, hep-ph/0210213 [INSPIRE].

[142] G. Corcella et al., *HERWIG 6: an event generator for hadron emission reactions with interfering gluons (including supersymmetric processes)*, *JHEP* **01** (2001) 010 [hep-ph/0011363] [INSPIRE].

[143] H. Yang et al., *Back-to-back azimuthal correlations in Z+jet events at high transverse momentum in the TMD parton branching method at next-to-leading order*, *Eur. Phys. J. C* **82** (2022) 755 [arXiv:2204.01528] [INSPIRE].

[144] A. Buckley et al., *Rivet user manual*, *Comput. Phys. Commun.* **184** (2013) 2803 [arXiv:1003.0694] [INSPIRE].

[145] A. Bermudez Martinez, F. Hautmann and M.L. Mangano, *TMD evolution and multi-jet merging*, *Phys. Lett. B* **822** (2021) 136700 [arXiv:2107.01224] [INSPIRE].

[146] A. Bermudez Martinez, F. Hautmann and M.L. Mangano, *Multi-jet physics at high-energy colliders and TMD parton evolution*, arXiv:2109.08173 [INSPIRE].

[147] A. Bermudez Martinez, F. Hautmann and M.L. Mangano, *Multi-jet merging with TMD parton branching*, *JHEP* **09** (2022) 060 [arXiv:2208.02276] [INSPIRE].

JHEP06(2025)192

[148] D. Antreasyan et al., *Dimuon Scaling Comparison at 44-GeV and 62-GeV*, *Phys. Rev. Lett.* **48** (1982) 302 [INSPIRE].

[149] NuSea collaboration, *Absolute Drell-Yan Dimuon Cross Sections in 800 GeV/c pp and pd Collisions*, hep-ex/0302019 [INSPIRE].

[150] J.C. Webb, *Measurement of continuum dimuon production in 800-GeV/C proton nucleon collisions*, Ph.D. thesis, New Mexico State University, U.S.A. (2003) [hep-ex/0301031] [INSPIRE].

[151] M.A. Ebert, I.W. Stewart and Y. Zhao, *Determining the Nonperturbative Collins-Soper Kernel From Lattice QCD*, *Phys. Rev. D* **99** (2019) 034505 [arXiv:1811.00026] [INSPIRE].

[152] M.A. Ebert, I.W. Stewart and Y. Zhao, *Renormalization and Matching for the Collins-Soper Kernel from Lattice QCD*, *JHEP* **03** (2020) 099 [arXiv:1910.08569] [INSPIRE].

[153] P. Shanahan, M. Wagman and Y. Zhao, *Collins-Soper kernel for TMD evolution from lattice QCD*, *Phys. Rev. D* **102** (2020) 014511 [arXiv:2003.06063] [INSPIRE].

[154] P. Shanahan, M. Wagman and Y. Zhao, *Lattice QCD calculation of the Collins-Soper kernel from quasi-TMDPDFs*, *Phys. Rev. D* **104** (2021) 114502 [arXiv:2107.11930] [INSPIRE].

[155] A. Avkhadiev, P.E. Shanahan, M.L. Wagman and Y. Zhao, *Determination of the Collins-Soper Kernel from Lattice QCD*, *Phys. Rev. Lett.* **132** (2024) 231901 [arXiv:2402.06725] [INSPIRE].

[156] A. Avkhadiev, P.E. Shanahan, M.L. Wagman and Y. Zhao, *Collins-Soper kernel from lattice QCD at the physical pion mass*, *Phys. Rev. D* **108** (2023) 114505 [arXiv:2307.12359] [INSPIRE].

[157] D. Bollweg, X. Gao, S. Mukherjee and Y. Zhao, *Nonperturbative Collins-Soper kernel from chiral quarks with physical masses*, *Phys. Lett. B* **852** (2024) 138617 [arXiv:2403.00664] [INSPIRE].

[158] D. Bollweg et al., *Transverse-momentum-dependent pion structures from lattice QCD: Collins-Soper kernel, soft factor, TMDWF, and TMDPDF*, arXiv:2504.04625 [INSPIRE].

[159] Lattice Parton collaboration, *Lattice-QCD Calculations of TMD Soft Function Through Large-Momentum Effective Theory*, *Phys. Rev. Lett.* **125** (2020) 192001 [arXiv:2005.14572] [INSPIRE].

[160] Lattice Parton (LPC) collaboration, *Nonperturbative determination of the Collins-Soper kernel from quasitransverse-momentum-dependent wave functions*, *Phys. Rev. D* **106** (2022) 034509 [arXiv:2204.00200] [INSPIRE].

[161] Lattice Parton (LPC) collaboration, *Lattice calculation of the intrinsic soft function and the Collins-Soper kernel*, *JHEP* **08** (2023) 172 [arXiv:2306.06488] [INSPIRE].

[162] Y. Li et al., *Lattice QCD Study of Transverse-Momentum Dependent Soft Function*, *Phys. Rev. Lett.* **128** (2022) 062002 [arXiv:2106.13027] [INSPIRE].

[163] M. Schlemmer et al., *Determination of the Collins-Soper Kernel from Lattice QCD*, *JHEP* **08** (2021) 004 [arXiv:2103.16991] [INSPIRE].

[164] H.-T. Shu et al., *Universality of the Collins-Soper kernel in lattice calculations*, *Phys. Rev. D* **108** (2023) 074519 [arXiv:2302.06502] [INSPIRE].

[165] MAP (Multi-dimensional Analyses of Partonic distributions) collaboration, *Unpolarized transverse momentum distributions from a global fit of Drell-Yan and semi-inclusive deep-inelastic scattering data*, *JHEP* **10** (2022) 127 [arXiv:2206.07598] [INSPIRE].

JHEP06(2025)192

[166] MAP (Multi-dimensional Analyses of Partonic distributions) collaboration, *Flavor dependence of unpolarized quark transverse momentum distributions from a global fit*, *JHEP* **08** (2024) 232 [arXiv:2405.13833] [INSPIRE].

[167] M. Bury et al., *PDF bias and flavor dependence in TMD distributions*, *JHEP* **10** (2022) 118 [arXiv:2201.07114] [INSPIRE].

[168] V. Moos, I. Scimemi, A. Vladimirov and P. Zurita, *Extraction of unpolarized transverse momentum distributions from the fit of Drell-Yan data at N^4LL*, *JHEP* **05** (2024) 036 [arXiv:2305.07473] [INSPIRE].

[169] F. Hautmann and D.E. Soper, *Parton distribution function for quarks in an s-channel approach*, *Phys. Rev. D* **75** (2007) 074020 [hep-ph/0702077] [INSPIRE].

[170] F. Hautmann and D.E. Soper, *Color transparency in deeply inelastic diffraction*, *Phys. Rev. D* **63** (2001) 011501 [hep-ph/0008224] [INSPIRE].

[171] M. Boglione and A. Simonelli, *Full treatment of the thrust distribution in single inclusive $e^+e^- \to h\ X$ processes*, *JHEP* **09** (2023) 006 [arXiv:2306.02937] [INSPIRE].

[172] S. Camarda, L. Cieri and G. Ferrera, *Drell-Yan lepton-pair production: qT resummation at N4LL accuracy*, *Phys. Lett. B* **845** (2023) 138125 [arXiv:2303.12781] [INSPIRE].

[173] S. Camarda, G. Ferrera and M. Schott, *Determination of the strong-coupling constant from the Z-boson transverse-momentum distribution*, *Eur. Phys. J. C* **84** (2024) 39 [arXiv:2203.05394] [INSPIRE].

[174] S. Camarda, L. Cieri and G. Ferrera, *Drell-Yan lepton-pair production: qT resummation at N3LL accuracy and fiducial cross sections at N3LO*, *Phys. Rev. D* **104** (2021) L111503 [arXiv:2103.04974] [INSPIRE].

[175] V. Bertone, G. Bozzi and F. Hautmann, *Perturbative RGE systematics in precision observables*, *Phys. Rev. D* **111** (2025) 074005 [arXiv:2407.20842] [INSPIRE].

[176] J. Isaacson, Y. Fu and C.-P. Yuan, *Improving resbos for the precision needs of the LHC*, *Phys. Rev. D* **110** (2024) 073002 [arXiv:2311.09916] [INSPIRE].

[177] T. Neumann and J. Campbell, *Fiducial Drell-Yan production at the LHC improved by transverse-momentum resummation at N4LLp+N3LO*, *Phys. Rev. D* **107** (2023) L011506 [arXiv:2207.07056] [INSPIRE].

[178] X. Chen et al., *Third-Order Fiducial Predictions for Drell-Yan Production at the LHC*, *Phys. Rev. Lett.* **128** (2022) 252001 [arXiv:2203.01565] [INSPIRE].

[179] W.-L. Ju and M. Schönherr, *The q_T and $\Delta\phi$ spectra in W and Z production at the LHC at $N^3LL'+N^2LO$*, *JHEP* **10** (2021) 088 [arXiv:2106.11260] [INSPIRE].

[180] M.A. Ebert, J.K.L. Michel, I.W. Stewart and F.J. Tackmann, *Drell-Yan q_T resummation of fiducial power corrections at N^3LL*, *JHEP* **04** (2021) 102 [arXiv:2006.11382] [INSPIRE].

[181] G. Billis, J.K.L. Michel and F.J. Tackmann, *Drell-Yan transverse-momentum spectra at N^3LL' and approximate N^4LL with SCETlib*, *JHEP* **02** (2025) 170 [arXiv:2411.16004] [INSPIRE].

[182] T. Becher and T. Neumann, *Fiducial q_T resummation of color-singlet processes at $N^3LL+NNLO$*, *JHEP* **03** (2021) 199 [arXiv:2009.11437] [INSPIRE].

JHEP06(2025)192